NAVAL POSTGRADUATE SCHOOL
Monterey, California

THESIS

DTIC
ELECTE
FEB 21 1992
S
B
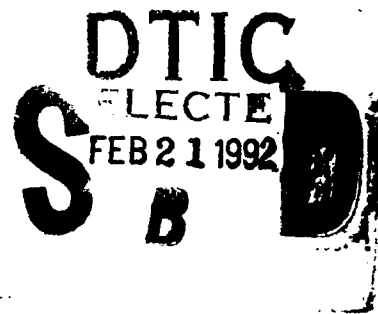
ACOUSTIC EMISSION FROM
SPECTRUM FATIGUE CRACKS
IN 7075 ALUMINUM

by

Wallace Dean Smith Jr.
Lieutenant, United States Navy

December, 1990

Thesis Advisor: Michael R. Gorman

Approved for public release; distribution is unlimited.

92-03911

92 2 14 049

REPORT DOCUMENTATION PAGE

Form Approved
OMB No. 0704-0188

1a REPORT SECURITY CLASSIFICATION UNCLASSIFIED	1b RESTRICTIVE MARKINGS
2a SECURITY CLASSIFICATION AUTHORITY	3. DISTRIBUTION/AVAILABILITY OF REPORT Approved for public release; distribution is unlimited.
2b DECLASSIFICATION/DOWNGRADING SCHEDULE	
4 PERFORMING ORGANIZATION REPORT NUMBER(S)	5. MONITORING ORGANIZATION REPORT NUMBER(S)

6a NAME OF PERFORMING ORGANIZATION Naval Postgraduate School	6b. OFFICE SYMBOL (If applicable) 31	7a. NAME OF MONITORING ORGANIZATION Naval Postgraduate School
6c. ADDRESS (City, State, and ZIP Code) Monterey, CA 93943-5000		7b ADDRESS (City, State, and ZIP Code) Monterey, CA 93943-5000

8a. NAME OF FUNDING/SPONSORING ORGANIZATION	8b. OFFICE SYMBOL (If applicable)	9. PROCUREMENT INSTRUMENT IDENTIFICATION NUMBER

8c. ADDRESS (City, State, and ZIP Code)	10 SOURCE OF FUNDING NUMBERS

	PROGRAM ELEMENT NO	PROJECT NO	TASK NO	WORK UNIT ACCESSION NO.

11. TITLE (Include Security Classification)

ACOUSTIC EMISSION FROM SPECTRUM FATIGUE CRACKS IN 7075 ALUMINUM

12. PERSONAL AUTHOR(S) Smith, Wallace D.

13a. TYPE OF REPORT Engineer's Thesis	13b. TIME COVERED FROM_____ TO_____	14. DATE OF REPORT (Year, Month, Day) December, 1990	15 PAGE COUNT 77

16. SUPPLEMENTARY NOTATION The views expressed in this thesis are those of the author and do not reflect the official policy or position of the Department of Defense or the U.S. Government.

17	COSATI CODES		18. SUBJECT TERMS (Continue on reverse if necessary and identify by block number)
FIELD	GROUP	SUB-GROUP	Aircraft fatigue, aging aircraft, crack growth, 7075 aluminum, spectrum loading, acoustic emission, plate waves.

19 ABSTRACT (Continue on reverse if necessary and identify by block number)

The E-2C Hawkeye, a U.S. Navy aircraft, has experienced problems with fatigue cracks in its wings. This problem was studied in the laboratory using a representative specimen under simulated flight loading. Acoustic emission monitoring was used to detect the stress pulses emitted during cracking. A new wave analysis technique was applied in order to distinguish extraneous noise from crack growth. This technique distinguishes between the extensional and flexural waves in thin aluminum plates. Extensional waves were found to correlate experimentally with waves from crack growth, while noise sources show different waveforms with lower frequencies. It was shown that acoustic emission provided early (crack length less than 0.01 inch) detection of fatigue cracking. This show promise for use in monitoring aircraft fatigue life.

20. DISTRIBUTION/AVAILABILITY OF ABSTRACT ☒ UNCLASSIFIED/UNLIMITED ☐ SAME AS RPT ☐ DTIC USERS	21. ABSTRACT SECURITY CLASSIFICATION UNCLASSIFIED	
22a. NAME OF RESPONSIBLE INDIVIDUAL Michael R. Gorman, Professor	22b TELEPHONE (Include Area Code) (408) 646-2074	22c. OFFICE SYMBOL AA/Go

DD Form 1473, JUN 86   Previous editions are obsolete.   SECURITY CLASSIFICATION OF THIS PAGE

S/N 0102-LF-014-6603

Acoustic Emission from Spectrum Fatigue Cracks
in 7075 Aluminum

by

Wallace D. Smith, Jr.
Lieutenant, United States Navy
B.S., United States Naval Academy, 1983

Submitted in partial fulfillment
of the requirements for the degree of

MASTER OF SCIENCE IN
AERONAUTICAL ENGINEERING

and

AERONAUTICS AND ASTRONAUTICS ENGINEER'S DEGREE

from the

NAVAL POSTGRADUATE SCHOOL
December, 1990

Author: _____
Wallace D. Smith Jr.

Approved by: _____
Michael R. Gorman, Thesis Advisor

_____
Indranath Dutta, Second Reader

_____
E. Roberts Wood, Chairman
Department of Aeronautics and Astronautics

_____
Dean of Faculty
and Graduate Studies

ABSTRACT

The E-2C Hawkeye, a U.S. Navy aircraft, has experienced problems with fatigue cracks in its wings. This problem was studied in the laboratory using a representative specimen under simulated flight loading. Acoustic emission monitoring was used to detect the stress pulses emitted during cracking. A new wave analysis technique was applied in order to distinguish extraneous noise from crack growth. This technique distinguishes between extensional and flexural waves in thin aluminum plates. Extensional waves were found to correlate experimentally with waves from crack growth, while noise sources show different waveforms with lower frequencies. It was shown that acoustic emission provided early (crack length < 0.01 in) detection of fatigue cracking. This shows promise for use in monitoring aircraft fatigue life.

Accession For

NTIS GRA&I	☑
DTIC TAB	☐
Unannounced	☐
Justification

By
Distribution/

Availability Codes

| Dist | Avail and/or Special |
| A-1 | |

iii

TABLE OF CONTENTS

I. INTRODUCTION

The E-2C Hawkeye is a fixed wing, propeller driven aircraft designed for use onboard fixed wing aircraft carriers of the U.S. Navy. Manufactured by Grumman Aerospace Corporation, the earliest variant of the E-2 first flew in 1961. The current 'C' variant is considerably newer, but the basic design remains the same. Through the years, the weight of avionics associated with performing the E-2C's mission of airborne early warning has increased. This, coupled with a growing emphasis on maximizing the useful life rather than replacing the airframe, has placed a great deal of interest on analyzing the fatigue life of the aircraft.

In 1984, after identifying fatigue critical areas on the aircraft, Grumman proposed to undertake a new, full-scale fatigue test of the E-2C [Ref. 1]. This was done in order to identify the effects of increased weight and to validate the expected useful life of 10,000 flight hours for the aircraft. A factor of safety of 2 was incorporated, which meant testing to 20,000 hours. A fatigue loading spectrum was developed based on a statistical analysis of previous flight performances and accelerometer readings from the aircraft. This data was then used in the fatigue testing of a full-scale airframe at the company's plant in Bethpage, New York.

In 1986, after 7,800 experimental flight hours, the fatigue test was stopped because cracks were observed to be developing in the wing center section (WCS) [Ref. 2]. The wing was torn down and

1

analyzed, and numerous modifications to the design were made to strengthen areas where fatigue cracking was occurring. After these changes were incorporated into a new WCS it was then installed in the airframe, replacing the damaged section. Testing recommenced in 1988. However, only the areas where the most severe fatigue cracking occurred had been redesigned and a problem area in the main beam web near wing station 49 remained unresolved. A 0.06" crack had developed in the earlier WCS during testing, resulting from the combined stress concentration effects of a fuel cell transfer cutout and a nearby hole in the web. The hole was one of the attachment holes used for securing the skin of the aircraft to the main beam. The location of this hole is shown in Figure I.1. The results of the Teardown Inspection Report identified this area as one of interest and in need of further study.

In order to assist the Naval Air Systems Command (NAVAIRSYSCOM) with this study, it was proposed to develop a model of the critical crack location and to fatigue the model under spectrum loading.

Acoustic emission (AE) techniques had been used previously to determine crack growth in 7075-T6 aluminum, from which the main beam was constructed. These studies had shown that AE testing techniques provide the ability to detect the crack initiation point, both by physical location and elapsed testing time. Additionally, recent studies that categorize waveforms by their source have provided new insights into understanding the process of acoustic emission. Experimental verification of these studies

should provide a new technique to increase AE sensitivity and solve the historical problems with noise discrimination during AE monitoring of fatigue. Based on the above, acoustic emission would be used to monitor the test in order to determine if crack initiation, defined as the presence of a crack 0.01" in length, could be identified.

In the present work, it is shown that acoustic emission from crack growth under spectrum fatigue can be identified by the extensional mode, which is characteristic of in-plane source motion. The noise waveforms are shown to have a characteristic shape and frequency content which are quite different from the crack AE. Thus the desired AE and noise are easily separated.

WCS   MAIN BEAM ASSEMBLY

AREA OF DETAIL

UP

OUTBOARD

FORWARD
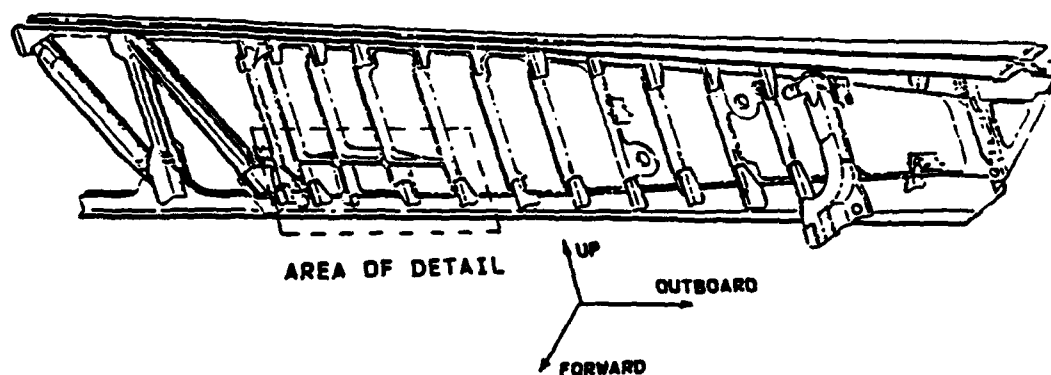
WCS, MAIN BEAM WEB AND LOWER CAPS, WS 32-57

CRACKS ON FATIGUE TEST TEARDOWN

FLIGHT HOURS = 7,800 HRS

#565
WEB, R/H
.005)

WS
57.5

#574
WEB, L/H
(.005)
AFT CAP, R/H
(.003)
FWD CAP, R/H
(.006)

WS
49

#575
WEB R/H
(.0506)
WEB, L/H
(.016)
AFT CAP R/H
(.007)

#606
WEB R/H
(.003)
AFT CAP, R/H
(.003)

#605
FWD CAP, R/H
(.003)

#593
FWD CAP, R/H
.006

WS
32

#607
WEB, R/H
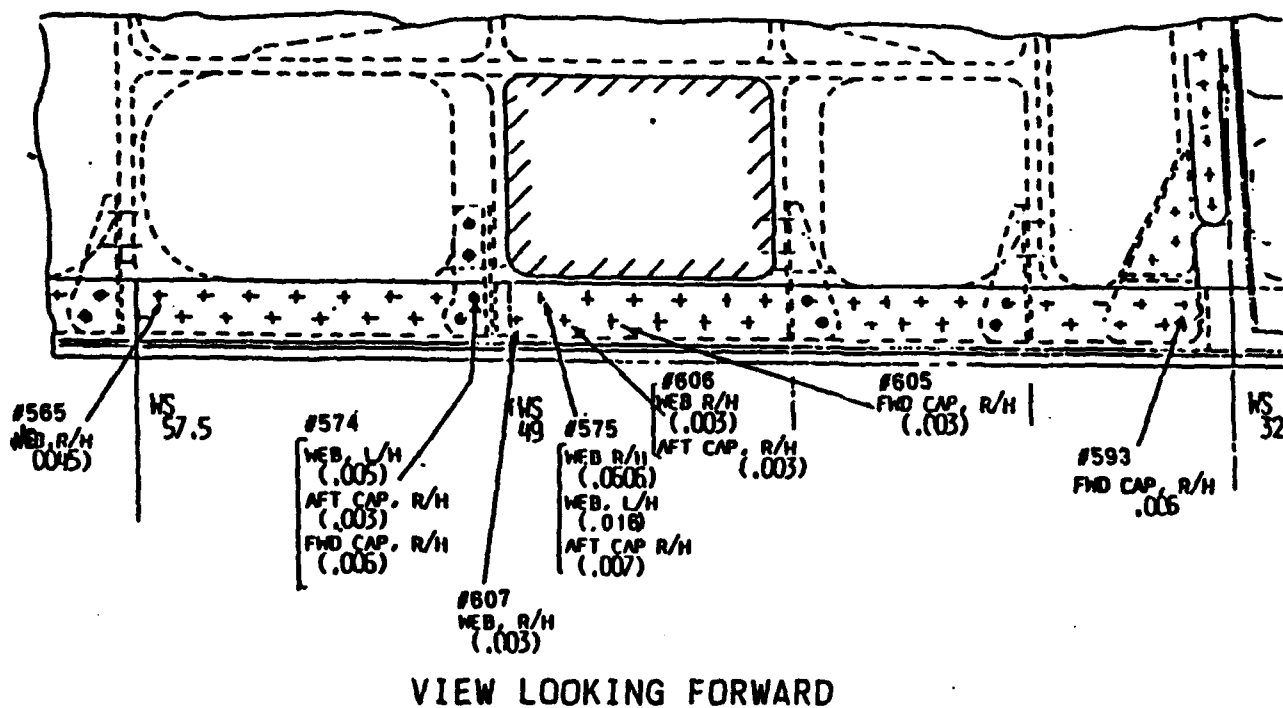(.003)

VIEW LOOKING FORWARD

FIGURE I.1:   Main Beam Diagram and Fatigue Crack Locations

4

II. REVIEW OF PREVIOUS WORK

Acoustic emission has evolved as a tool in non-destructive testing (NDT) over the past twenty years. Its application to fatigue in structural materials has been limited because the large amount of extraneous noise created in a typical test setup, drowns out the signals from the cracks. Accordingly, most of the efforts to date have been devoted to either eliminating or discriminating the noise from the actual fatigue cracking signals.

Some of the initial work done in the field of stress wave characterization was performed by Gerberich and Hartblower [Ref. 3]. They utilized a bandpass filter of 2 to 6 KHz to filter out low frequency machine noise during static testing. The remaining signals were characterized as stress waves created by slow crack growth. They found that the crack growth rate correlated linearly with the stress wave amplitude in 7075-T6 aluminum and other metals. Gillis [Ref. 4] was among the first to postulate that the stress waves might have their origin in dislocation movement. Tetelman [Ref. 5] observed that brittle materials were more active acoustically than ductile ones and hypothesized that this was due to the difference in dislocation mechanisms in the materials. However, it was not until recently that McBride et al. [Ref. 6] finally identified experimentally the fracture of intermetallic inclusions in 7075-T6 as the source of acoustic emission. It was also shown that the maximum amplitude of a crack growth signal was

about 10 times smaller than those for crack rubbing and fretting, thus highlighting the importance of noise discrimination.

Early work on the use of AE to detect fatigue damage in metals identified numerous means to isolate fatigue crack emission. Smith and Morton [Ref. 7] used three methods to decrease or discriminate against noise in a fatigue test. Firstly, noise damping interfaces were used to isolate the specimen acoustically. Secondly, the detection system was gated to permit listening only during the top 10% of loading, when most cracking was suspected to occur. Thirdly, spatial filtering was used to eliminate signals whose time of arrival indicated they originated outside the area of interest on the specimen. In this technique, transducers are placed between the noise source and the transducers being used to detect the acoustic emission from the crack. Signals from two, 155 KHz resonant transducers were amplified by 100 dB and then filtered using 30 KHz low pass filters. The results of their experiments with spatial filtering proved to be most effective with crack growth rates in aluminum of 5×10^{-6} inch per cycle or less.

Harris and Dunegan [Ref. 8] attempted to classify cracking from noise in 7075-T6 aluminum by using rise time discrimination. The rise time is defined as the time it takes for the amplified signal to reach its maximum voltage (see Section III.D). They noted that crack growth was usually associated with a signal that rose quickly to peak amplitude (fast rise time). Crack closure and fretting, on the other hand, were more likely to be slow rise time events observed even in tension-tension loading. Load cycle

gating, 100 to 300 KHz band-pass filters (centered on the resonant frequency of the transducers) and high gains of 60 to 80 dB for increased sensitivity were used. The frequency of load cycling was found to increase the amount of AE events by increasing crack growth rate. The use of rise time discrimination was confirmed by Morton et al. [Ref. 9, 10], who, by comparing aluminum and magnesium alloys, observed that material characteristics, such as heat treatment and deformation mechanisms, played a large part in crack growth AE rate.

Singh and Davis [Ref. 11] were less supportive of the stand alone viability of AE based on their tests of fatigue crack growth in 7075-T6 aluminum. However, they did attempt an early, theoretical characterization of the stress waves by frequency and source. Most notable was their analysis that the acoustic emission stress waves originate at dislocation/defect sources and travel on the surface as compressional or shear waves. Darlow et al. [Ref. 12] agreed with this characterization of AE waves and attempted to identify crack initiation in titanium. Titanium was found to have AE signals of significantly higher amplitude than machine noise, due to the brittle nature of the material. Beginning with static testing and then progressing to low cycle fatigue, the amount of AE was observed to increase with crack growth rate and stress concentration factors.

Wadin and Dunegan [Ref. 13] expanded on techniques of spatial and bandpass filtering and developed a discrimination scheme based on the width of the received signal pulse. The width of the signal

7

is defined as the amount of time the signal remains above the reception threshold. They noted that the widths of crack growth signal pulses were shorter than those due to noise signals during fatigue of 7075-T6 aluminum. Bailey et al. [Ref. 14] successfully monitoring crack growth in the same material during low cycle fatigue using only high pass filtering above 500 KHz. Lindley et al. [Ref. 15] used bandpass filtering and load cycle gating to achieve a similar success in monitoring crack growth, also in 7075-T6 aluminum.

Peapell and Topp [Ref. 16] and Provan [Ref. 17] have remarked on the difficulty of characterizing signals in metals, where reflections of the waves tended to complicate the signals. Still, both Bathias [Ref. 18] and Houssay-Eman and Bassim [Ref. 19] felt that AE could identify the three stages of plastic deformation in metals, namely, dislocation movement, formation of microcracks, and crack initiation.

Additional work on the fatigue of aluminum utilized one or all of the noise discrimination techniques mentioned above. These include: bandpass filtering, load cycle gating, spatial discrimination, discrimination by parameter (i.e. ring down count, rise time, pulse width, amplitude or frequency content have all been used to some degree in testing) and damping of extraneous background and machine noises. The minimum detectable crack length in aluminum during fatigue has varied to include values of 0.01" [Ref. 20], 0.03" [Ref. 14] and 0.05" [Ref. 21].

Recently, the focus of work in AE has shifted from examining waveform parameters to understanding the waveforms themselves. Gorman [Ref. 22] has shown that the AE stress waves in thin plates of aluminum may be separated into their extensional and flexural components. This requires the use of broadband transducers in order to accurately capture the waveform frequencies and amplitudes.

III. WAVE THEORY

Wave theory as applied to this thesis concerns three general areas. First, the application of wave motion in elastic solids as applied to thin plates was considered. Second, the concept of determining the linear location of the source of a wave by measuring the difference in arrival times at separate sensors was studied. Finally, the acoustic emission terminology as accepted within the AE industry was reviewed and applied to the above.

Stress waves, or acoustic emission events, in a sheet of metal are observed to be in the form of plate waves. In thin plates, or those where thickness is relatively small compared to the other two dimensions of length and width, these waves are found to be in the form of extensional and flexural modes. An AE event will usually cause both modes to be excited. This is because of a coupling between them due to Poisson's ratio. However, usually only one mode will be the largest, primary mode.

A. FLEXURAL WAVE

To derive the equations of motion for a flexural wave in a thin plate, an infinite plate of thickness, h, is considered, as in Figure III.1 [Ref. 23]. A differential element, h dx dy, is subjected to shear forces per unit length, Q, bending and twisting moments per unit length, M, and external loads per unit area, q. Only the force equation of motion in the z-direction and the two moment equations of motion about the x- and y-axis are considered.
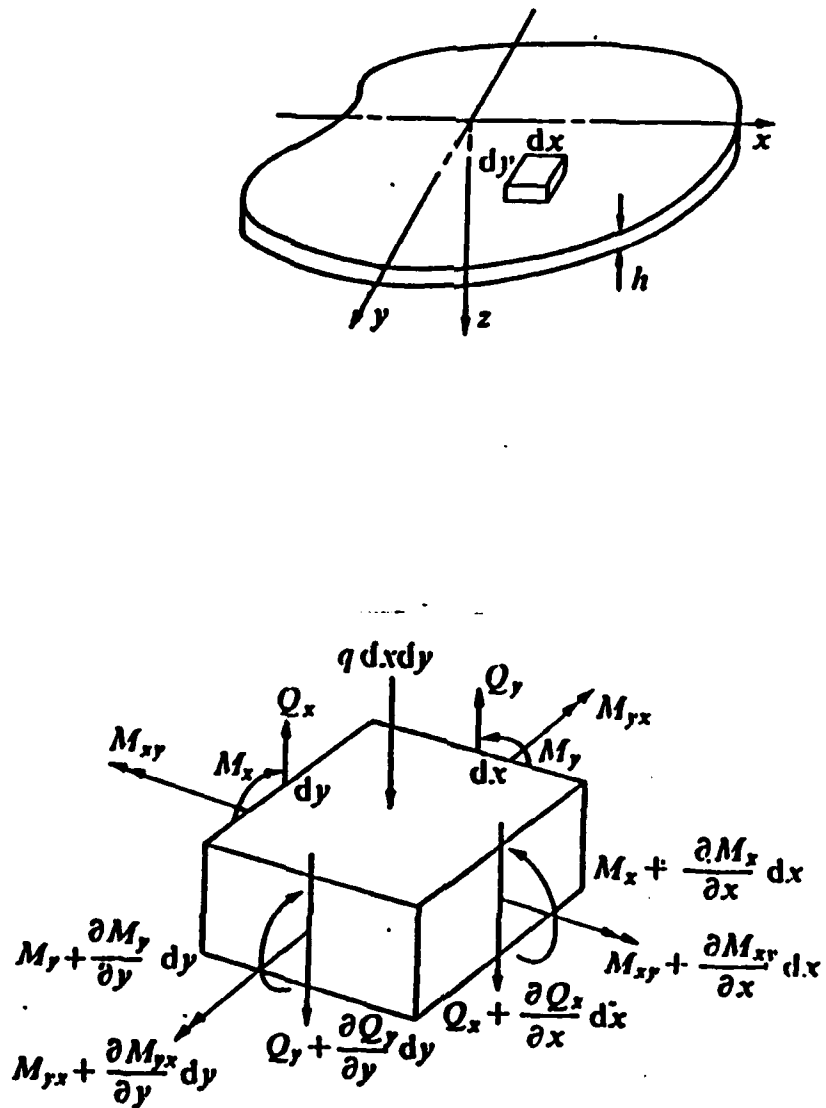
10

Figure III.1: Infinite Plate and Element Forces

The others equations constitute the trivial case. By neglecting rotary-inertia effects and higher order contributions from q to the moments, the resulting equations of motion are given as

$$-Q_x dy + (Q_x + \frac{\partial Q_x}{\partial x} dx) dy - Q_y dx + (Q_y + \frac{\partial Q_y}{\partial y} dy) dx + q dx dy = \rho h dx dy \frac{\partial^2 w}{\partial t^2}, \quad (1)$$

$$(M_y + \frac{\partial M_y}{\partial y} dy) dx - M_y dx + M_{xy} dy - (M_{xy} + \frac{\partial M_{xy}}{\partial x} dx) dy - Q dx dy = 0 \quad (2)$$

and

$$(M_z + \frac{\partial M_x}{\partial x} dx) dy - M_x dy + (M_{yx} + \frac{\partial M_{yx}}{\partial y} dy) dx - M_{yx} dx - Q_x dy dx = 0. \quad (3)$$

Canceling like terms, these reduce to

$$\frac{\partial Q_x}{\partial x} + \frac{\partial Q_y}{\partial y} + q = \rho h \frac{\partial^2 w}{\partial t^2}, \quad (4)$$

$$\frac{\partial M_y}{\partial y} - \frac{\partial M_{xy}}{\partial x} - Q_y = 0 \quad (5)$$

and

$$\frac{\partial M_x}{\partial x} + \frac{\partial M_{yx}}{\partial y} - Q_x = 0. \quad (6)$$

Equations (5) and (6) are solved for Q_x and Q_y and substituting into equation (4). From this, the following equation of motion in terms of moments is obtained

$$\frac{\partial^2 M_x}{\partial x^2} + \frac{\partial^2 M_{yx}}{\partial x \partial y} - \frac{\partial^2 M_{xy}}{\partial y \partial x} + \frac{\partial^2 M_y}{\partial x^2} + q = \rho h \frac{\partial^2 w}{\partial t^2} \, . \tag{7}$$

The kinematics of plate deformation are now considered and the differential element reconsidered in Figure III.2. By introducing the assumption that plane sections remain plane and perpendicular to the mid-plane, the normal strains are given as

$$\varepsilon_x = \frac{z}{r_x} \quad \text{and} \quad \varepsilon_y = \frac{z}{r_y} \, . \tag{8}$$

Here r_x and r_y define radii of curvature. For small deflections and slopes, the curvature may be approximated by $-\delta^2 w/\delta x^2$ and $-\delta^2 w/\delta y^2$. This yields

$$\varepsilon_x = -z \frac{\partial^2 w}{\partial x^2} \quad \text{and} \quad \varepsilon_y = -z \frac{\partial^2 w}{\partial y^2} \, . \tag{9}$$

The engineering shear strain is defined as

$$\gamma_{xy} = \frac{\partial u}{\partial y} + \frac{\partial v}{\partial x} \, . \tag{10}$$

Here displacements are given by $u = -z \delta w/\delta x$ and $v = -z \delta w/\delta y$, so that

$$\gamma_{xy} = -2z \frac{\partial^2 w}{\partial x \partial y} \, . \tag{11}$$

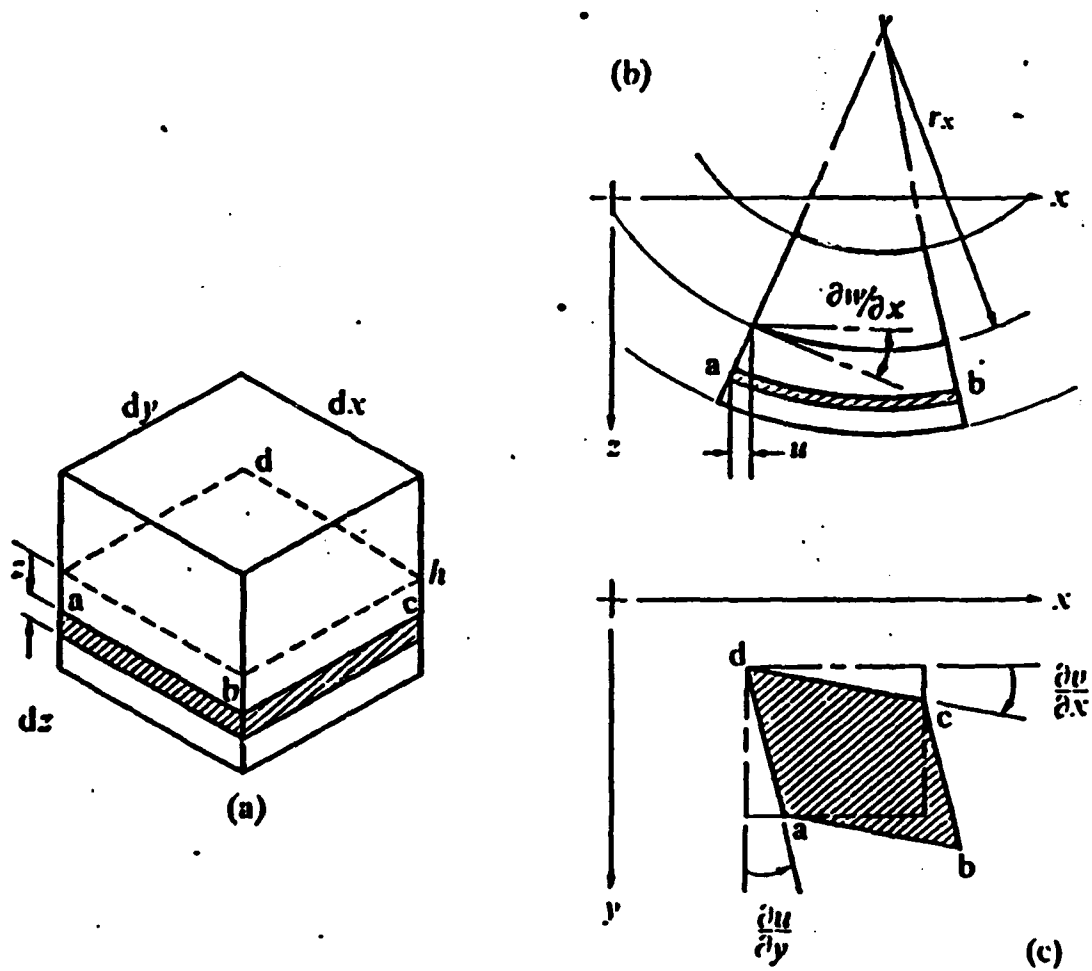From Hooke's law the stresses are defined as

Figure III.2: Differential Plate Element

$$\sigma_x = \frac{E}{1-v^2} \left(\varepsilon_x + v\varepsilon_y \right) = -\frac{Ez}{1-v^2} \left(\frac{\partial^2 w}{\partial x^2} + v\frac{\partial^2 w}{\partial y^2} \right), \qquad (12)$$

$$\sigma_y = \frac{E}{1-v^2} \left(\varepsilon_y + v\varepsilon_x \right) = -\frac{Ez}{1-v^2} \left(\frac{\partial^2 w}{\partial y^2} + v\frac{\partial^2 w}{\partial x^2} \right) \qquad (13)$$

and

$$\tau_{xy} = G\gamma_{xy} = -2Gz\frac{\partial^2 w}{\partial x \partial y}. \qquad (14)$$

These equations are now used to evaluate the bending and twisting moments. The bending moment on face h dy due to σ_x is given by

$$M_x dy = \int_{-h/2}^{h/2} z\sigma_x dy dx \qquad (15)$$

or

$$M_x = \int_{-h/2}^{h/2} z\sigma_x dz. \qquad (16)$$

By substituting the expression for σ_x in equation (12) into equation (16) and carrying out the integration, the following is obtained

$$M_x = -D\left(\frac{\partial^2 w}{\partial x^2} + v\frac{\partial^2 w}{\partial y^2} \right). \qquad (17)$$

15

Here the flexural rigidity, D, is defined as

$$D = \frac{Eh^3}{12(1-v^2)}.$$ (18)

Similarly, for M_y

$$M_y = -D\left(\frac{\partial^2 w}{\partial y^2} + v\frac{\partial^2 w}{\partial x^2}\right).$$ (19)

The equation for M_{xy} is slightly different, requiring a negative sign to compensate the positive shear stress for the sign convention established

$$M_{xy} = -\int_{-h/2}^{h/2} z\tau_{xy}dz.$$ (20)

Upon evaluation, this yields

$$M_{xy} = D(1-v)\frac{\partial^2 w}{\partial x\partial y}.$$ (21)

Since $M_{xy} = -M_{yx}$, the equation of motion (7) may now be written as

$$D\left(\frac{\partial^4 w}{\partial x^4} + 2\frac{\partial^4 w}{\partial^2 x\partial^2 y} + \frac{\partial^4 w}{\partial y^4}\right) - q = -\rho h\frac{\partial^2 w}{\partial t^2}.$$ (22)

Here the expression inside the parenthesis can be reduced to

16

$$\frac{\partial^4 w}{\partial x^4} + 2\frac{\partial^4 w}{\partial x^2 \partial y^2} + \frac{\partial^4 w}{\partial y^4} = (\frac{\partial^2}{\partial x^2} + \frac{\partial^2}{\partial y^2})(\frac{\partial^2 w}{\partial x^2} + \frac{\partial^2 w}{\partial y^2}) = \nabla^2 \nabla^2 w. \qquad (23)$$

Thus, the governing equation for the flexural wave in a thin plate is given as

$$D\nabla^4 w(x,y,t) + \rho h\frac{\partial^2 w(x,y,t)}{\partial t^2} = q(x,y,t). \qquad (24)$$

To solve this equation, consider a solution as a harmonic wave of the form

$$w = Ae^{i(kr-\omega t)}. \qquad (25)$$

This yields, for the various terms

$$\nabla^2 w = -Ak^2 e^{i(kr-\omega t)}, \qquad (26)$$

$$\nabla^4 w = Ak^4 e^{i(kr-\omega t)} \qquad (27)$$

and

$$\frac{\partial^2 w}{\partial t^2} = -A\omega^2 e^{i(kr-\omega t)}. \qquad (28)$$

By letting the external load q equal zero and substituting into equation (24), the following is obtained

$$DAk^4 e^{i(kr-\omega t)} - \rho hA\omega^2 e^{i(kr-\omega t)} = 0. \qquad (29)$$

17

This provides the frequency-wavenumber expression for flexural plate waves

$$\omega = k^2 \sqrt{\frac{D}{\rho h}} \, . \tag{30}$$

and, for omega=kc, the dispersion relation

$$c = k \sqrt{\frac{D}{\rho h}} \, . \tag{31}$$

B. EXTENSIONAL WAVE

For the extensional case [Ref. 24], the governing equations may be derived from the equations of motion

$$\frac{\partial \sigma_{ij}}{\partial x_j} + F_i = \rho \frac{\partial^2 u_i}{\partial t^2} \tag{32}$$

where a sum over repeated indices is intended. Assuming plane stress, $\sigma_z = \tau_{xz} = \tau_{yx} = 0$, and neglecting out-of-plane body forces, $F_z = 0$, these reduce to

$$\frac{\partial \sigma_x}{\partial x} + \frac{\partial \tau_{xy}}{\partial y} + F_x = \rho \frac{\partial^2 u}{\partial t^2} \tag{33}$$

and

$$\frac{\partial \tau_{yx}}{\partial x} + \frac{\partial \sigma_y}{\partial y} + F_y = \rho \frac{\partial^2 v}{\partial t^2} \, . \tag{34}$$

Hooke's law is given as,

$$\sigma_{ij} = \lambda \varepsilon_{kk} \delta_{ij} + 2\mu \varepsilon_{ij} \, . \tag{35}$$

By setting $\sigma_z = \sigma_{33} = 0$, it may be seen that $\epsilon_z = \epsilon_3$ is related to $\epsilon_x + \epsilon_y$ by

$$\varepsilon_3 = -\frac{\lambda}{\lambda + 2\mu} \frac{\partial u_k}{\partial x_k} \, . \tag{36}$$

Hence equation (35) can be rewritten as

$$\sigma_{ij} = \frac{2\mu\lambda}{\lambda + 2\mu} \frac{\partial u_k}{\partial x_k} \delta_{ij} + \mu \left(\frac{\partial u_i}{\partial x_j} + \frac{\partial u_j}{\partial x_i} \right) \, . \tag{37}$$

For conditions of plane stress this becomes

$$\sigma_x = \frac{2\mu\lambda}{\lambda + 2\mu} \left(\frac{\partial u}{\partial x} + \frac{\partial v}{\partial y} + \frac{\partial w}{\partial z} \right) + \mu \left(2 \frac{\partial u}{\partial x} \right) \, , \tag{38}$$

$$\tau_{xy} = \tau_{yx} = \mu \left(\frac{\partial u}{\partial y} + \frac{\partial v}{\partial x} \right) \tag{39}$$

and

$$\sigma_y = \frac{2\mu\lambda}{\lambda + 2\mu} \left(\frac{\partial u}{\partial x} + \frac{\partial v}{\partial y} + \frac{\partial w}{\partial z} \right) + \mu \left(2 \frac{\partial v}{\partial y} \right) \, . \tag{40}$$

19

Here Lame's constants are given in terms of elastic modulus and Poisson's ratio as

$$\lambda = \frac{E\nu}{(1+\nu)(1-2\nu)} \tag{41}$$

and

$$\mu = \frac{E}{2(1+\nu)} . \tag{42}$$

Lame's constants are inserted into equations (38) through (40) and the resulting equations differentiated. Upon substitution into equations (33) and (34), the governing equations for the extensional mode follow

$$\frac{\partial^2 u}{\partial x^2} + \frac{1-\nu}{2} \frac{\partial^2 u}{\partial y^2} + \frac{1+\nu}{2} \frac{\partial^2 v}{\partial x \partial y} - \frac{(1-\nu^2)\rho}{E} \frac{\partial^2 u}{\partial t^2} \tag{43}$$

$$\frac{\partial^2 v}{\partial y^2} + \frac{(1-\nu)}{2} \frac{\partial^2 v}{\partial x^2} + \frac{(1+\nu)}{2} \frac{\partial^2 u}{\partial x \partial y} - \frac{(1-\nu^2)\rho}{E} \frac{\partial^2 v}{\partial t^2} \tag{44}$$

Again, a solution of the form

$$u = A e^{i(kx-\omega t)} \quad and \quad v = 0 \tag{45}$$

is assumed. When this is substituted into the governing equations, the frequency-wavenumber expression for extensional plate waves is given as

20

$$\omega = k \sqrt{\frac{E}{\rho (1 - v^2)}} .$$ (46)

By substituting for omega=kc,

$$c = \sqrt{\frac{E}{\rho (1 - v^2)}}$$ (47)

it can be seen that the mode is dispersionless (velocity is independent of wave number k). Thus it is seen that the velocity of the extensional wave is independent of frequency. Therefore the dispersionless, extensional wave more accurately preserves the waveform generated by an event than the flexural wave does. The concept of linear location of an AE source requires an accurate measurement of arrival times of the stress pulse at known locations. Consequently, the non-dispersive nature of the extensional wave provides a better waveform on which to trigger for the time of arrival locating information.

C. LINEAR LOCATION

By measuring the difference in arrival times of a wave with a known velocity at two or more sensors at known locations, locating data for the AE source may be obtained. For linear location, as used in this experiment, the concept is a simple one, as illustrated in Figure III.3. Two transducers are placed on either side of an AE source with a known distance, D, between them.
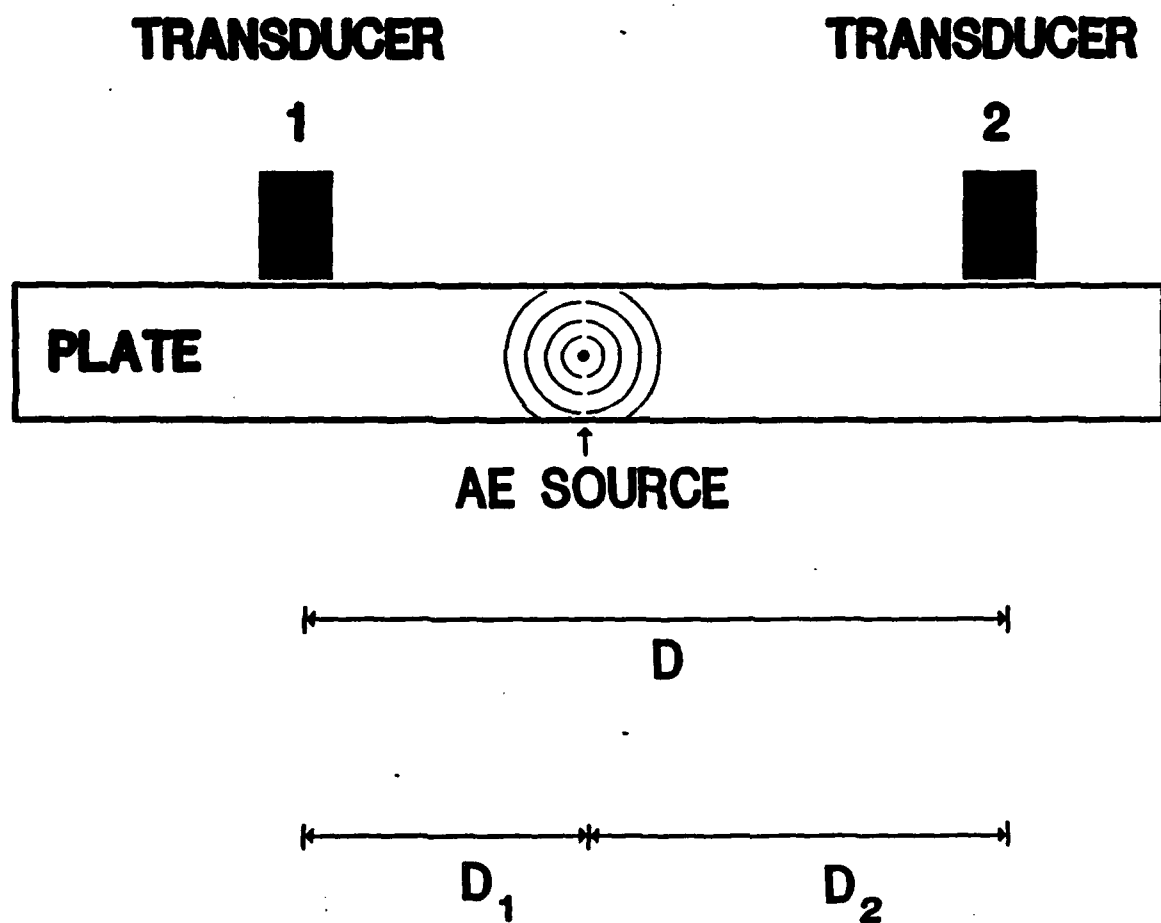
TRANSDUCER 1

TRANSDUCER 2

PLATE

AE SOURCE

D

D_1

D_2

Figure III.3: Linear Location Setup

Given the definition of wave speed (c) and distance between transducers (D)

$$\Delta t_{max} = \frac{D}{c} \qquad (48)$$

and

$$D_1 + D_2 = D. \qquad (49)$$

For time of arrival at sensor 1 as t_1 and at sensor 2 as t_2

$$\Delta t = t_2 - t_1. \qquad (50)$$

Rearranging this expression

$$\Delta t = \frac{(D - D_1) - D_1}{c} \qquad (51)$$

$$\Delta t = \frac{D}{c} - \frac{2D_1}{c}. \qquad (52)$$

The maximum time of arrival difference between two sensors is required. It may be calculated by using the wave propagation speed in the medium and the distance between the sensors. It may also be determined experimentally using an AE source (such as lead breaks) on a line passing through the two sensors and outside the region between them.

From these it is possible to develop an equation for the distance of the source from transducer 1 (D_1) in terms of maximum

time of arrival difference (Δt_{max}), measured time of arrival difference (Δt), and distance between the two sensors by substituting for t_1 and t_2 as follows:

$$D_1 = \frac{(\frac{D}{c} - \Delta t)}{2} c \tag{53}$$

$$D_1 = \frac{(\Delta t_{max} - \Delta t)}{2} \frac{D}{\Delta t_{max}} . \tag{54}$$

$$\Delta t = \frac{D_2 - D_1}{c} \tag{55}$$

D. ACOUSTIC EMISSION TERMINOLOGY

The use of AE in the past has been confined primarily to statistical analysis of events. An event is defined as one acoustical pulse. As a crack starts and grows under stress many events, or pulses, are detected. A typical pulse is shown in Figure III.4. Both the signal and the threshold of the AE analyzer are shown in voltage versus time. The waveform has traditionally been described in terms of parameters. Peak amplitude of the pulse indicates the maximum signal strength reached. Rise time is defined as the time from trigger (first threshold crossing) to peak amplitude. Fast rise time is considered to be a relatively short, or high slope line. Ringdown counts are defined as the number of times the signal exceeds the preset threshold. Event duration is the time between the first and last threshold crossing.
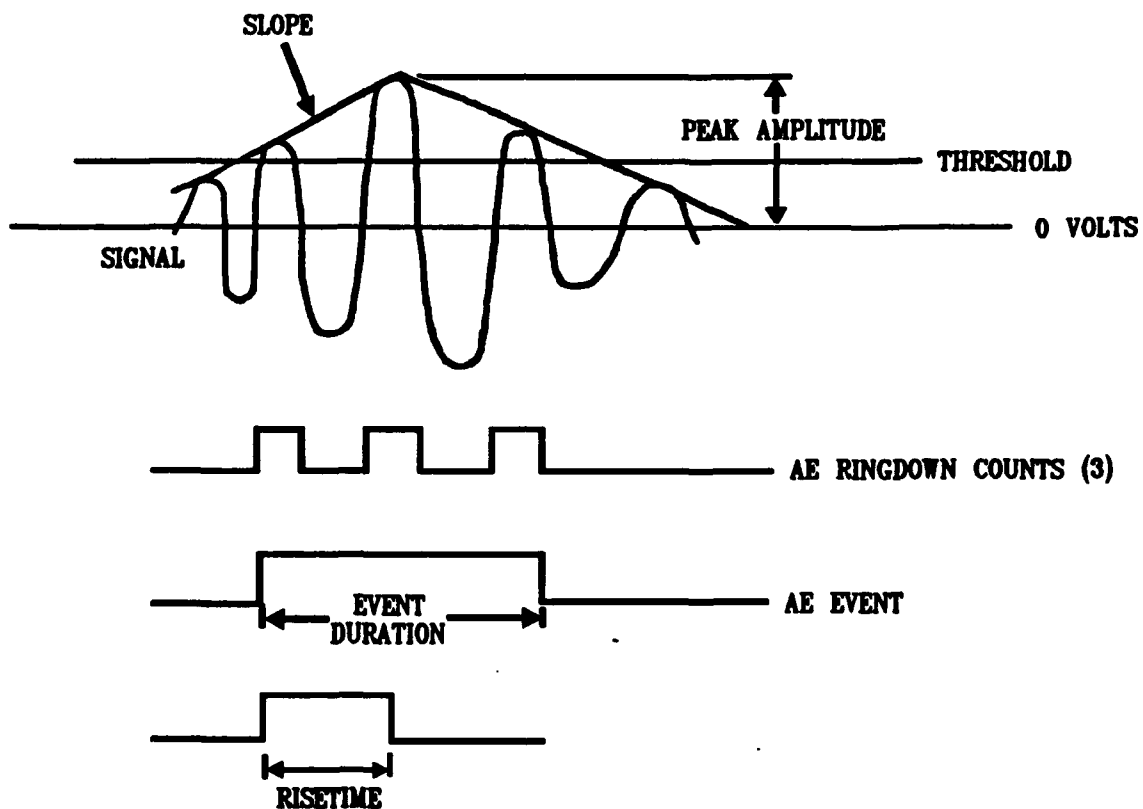
Figure III.4: Typical AE Signal

25

In the past, as discussed in Section II, it has been observed that fast rise time, low ringdown count, short event duration events have been associated with crack growth. Conversely, slow rise time, high ringdown count, long event duration events have been characteristic of extraneous noise or crack fretting. It has been proposed that, due to the in-plane source motion, crack growth should be primarily composed of extensional waves [Ref. 22] which, due to their non-dispersive nature, have fast rise times and short event durations. Extraneous noise, on the other hand, may be primarily composed of flexural waves which, due to their dispersive nature, have slow rise times and long event durations. These differences are further amplified since the signal due to noise can be stronger than the extensional signal from cracking. This new approach to interpreting traditional AE data now had to be tested experimentally.

IV. INSTRUMENTATION

A. EXPERIMENTAL SET-UP

Specimen testing was done in the Non-Destructive Evaluation (NDE) Lab of the Aeronautical Engineering Department at the U.S. Naval Postgraduate School. The basic concept was to create a specimen which modelled the stresses in the main beam web, critical crack area. The specimen was tested under static and fatigue loading using a Materials Testing System (MTS) Model 810 testing machine. Each test was monitored using acoustic emission and time-lapse, video microscopy. The digitized load, AE and observed crack length were recorded and correlated by synchronizing them with the recorded elapsed time. The entire setup is shown as a block diagram in Figure IV.1 and explained below.

B. SPECIMEN SELECTION AND SPECTRUM LOADING

A 4" wide by 14" long, 0.125" thick aluminum specimen was used to model the critical crack area using a 1:1 scale. It modelled the lower portion of the both the main beam web and fuel cell cutout, and the critical attachment hole. The specimen is shown in Figure IV.2. To reproduce the stress conditions in the vicinity of wing station 49, the actual stress levels in the full-scale test article were obtained. This allowed the area of interest to be studied and sized using finite-element modeling.
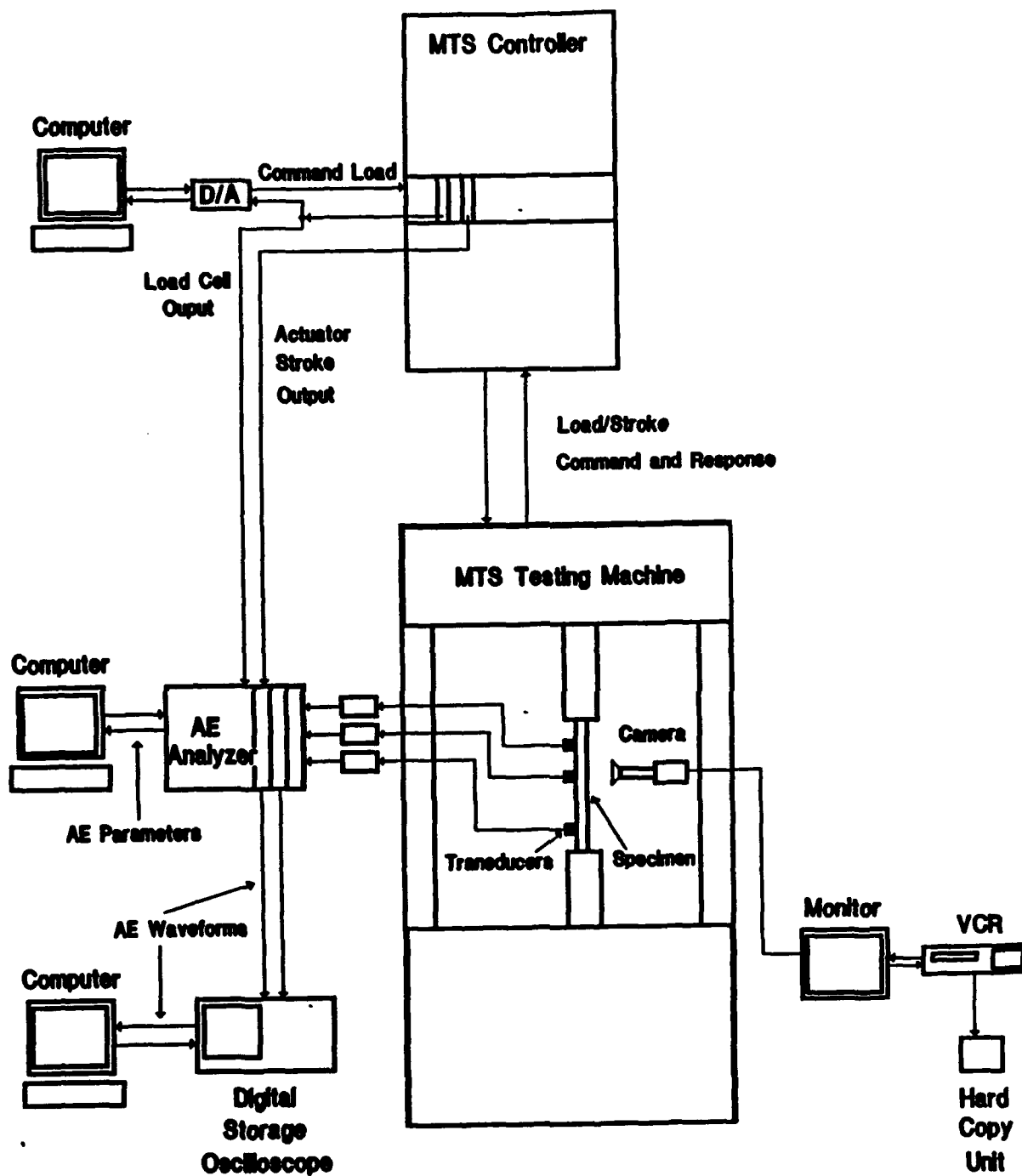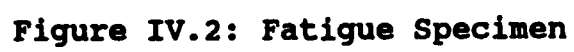
Figure IV.1: System Setup

28

Figure IV.2: Fatigue Specimen

During selection of the specimen several simplifying assumptions were made. Firstly, it was assumed that the region was under a state of uniaxial stress. This appeared to be a reasonable assumption due to two conditions: (a) the main beam web was relatively large in size when compared to the region of interest, located near the outer edge of the web; and (b) the bending stresses due to flight and landing loads were large in magnitude when compared with the smaller skin loads in the region. Thus the bending loads at the outer edge of the web could be approximated as a uniform, uniaxial stress.

Secondly, it was assumed that the region was in a state of plane stress. This was reasonable due to a relatively thin web (0.143") in relation to the length and height of the beam (310" and 21.35" respectively). This assumption is in consonance with the plate wave theory discussed earlier.

The finite-element program GIFTS was used to compute the stresses in the model. GIFTS (Graphical Interactive Finite-element Total System) is a linear, finite-element programming package resident on the VAX 11/780 computer in the Aeronautical Engineering Department. It was used to construct a 900-element model of one quarter of the specimen. An initial stress analysis of the specimen is shown in Figure IV.3 for an applied stress of 20,000 psi. Contours of constant stress are shown, correlating to the numerical value at right. When the attachment hole was added, the stress concentration factor about the attachment hole was
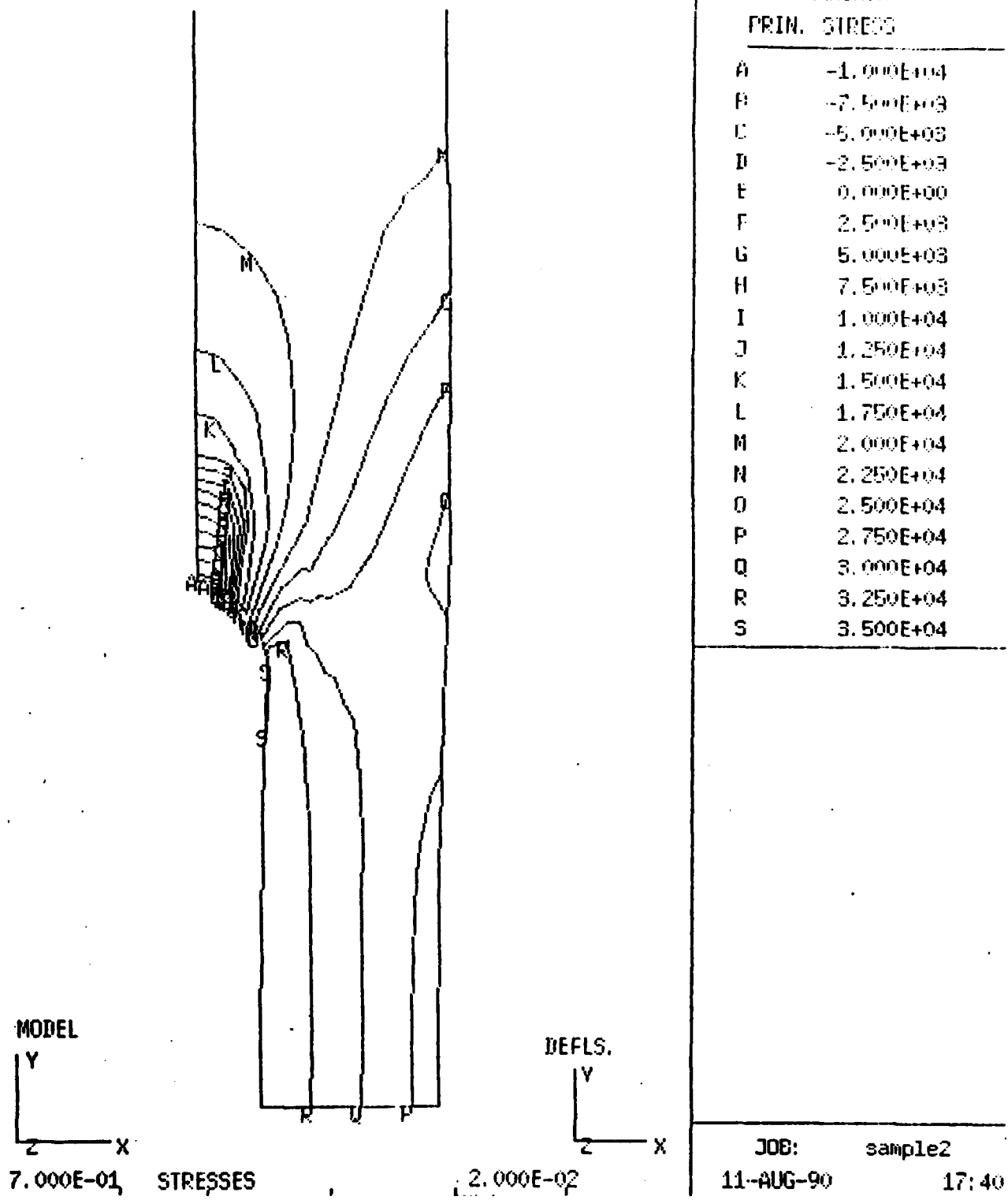
PRIN. STRESS	
A	-1.000E+04
B	-7.500E+03
C	-5.000E+03
D	-2.500E+03
E	0.000E+00
F	2.500E+03
G	5.000E+03
H	7.500E+03
I	1.000E+04
J	1.250E+04
K	1.500E+04
L	1.750E+04
M	2.000E+04
N	2.250E+04
O	2.500E+04
P	2.750E+04
Q	3.000E+04
R	3.250E+04
S	3.500E+04

MODEL

7.000E-01   STRESSES

DEFLS.

2.000E-02

JOB: sample2

11-AUG-90   17:40

Figure IV.3:   GIFTS Stress Analysis of Model

31

calculated to be 2.35 [Ref. 25]. This was confirmed using GIFTS and is shown in enlarged detail in Figure IV.4.

This model was compared with finite-element stress computations and actual strain gauge data from the full-scale article, provided by Grumman and shown in Figures IV.5 and IV.6. Figure IV.5 shows the finite-element model's principal stress directions and values for the full-scale model. Figure IV.6 shows the actual strain gauge locations and stress (in kpsi) for the area of interest on the full-scale, fatigue article. After a comparison of the specimen and full-scale model results, a slight modification was made to widen the initial slot size in the center of the specimen. This provided a greater inward curve of the stress contours in the ligament, as seen in the larger, Grumman model. The effect of widening the slot on stress contours is shown in Figure IV.7 (a) through (c). The stress contour values used are shown in (d). The slot width was limited from further expansion by the size of the grips on the MTS testing machine, which had a maximum specimen width of 4". However, the stress contours in the region between the attachment hole and the cutout showed a high correlation with stress levels in the actual aircraft.

The specimens were constructed from 7075-T6 sheet aluminum (bare) of 0.125" thickness. This is the same material as the main beam web, only slightly thinner. Since the assumption of plane stress had already been made, it was only necessary to match the stress levels in the full-scale article. Care was also taken in preparation of the specimens. They were cut from the center of the
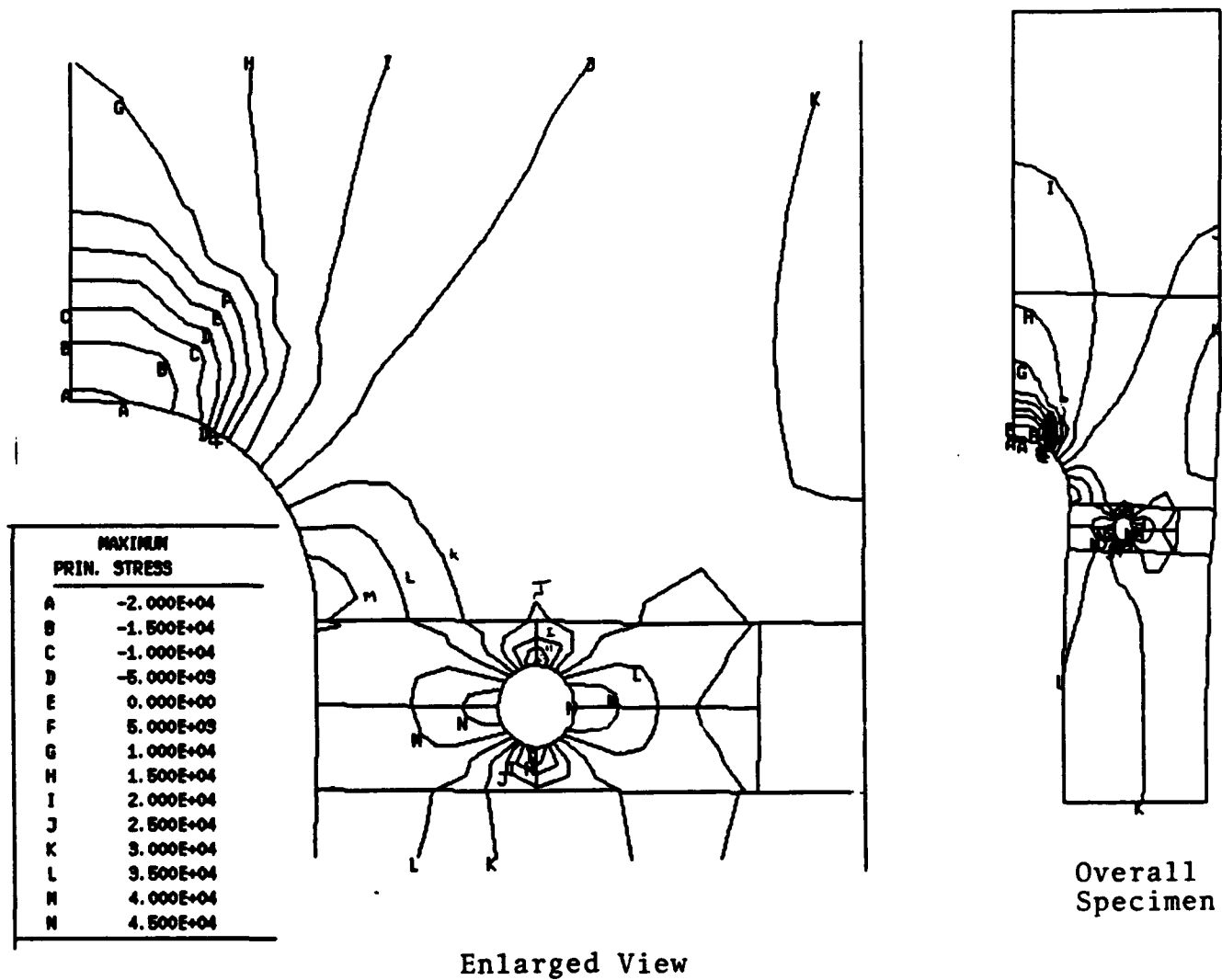
32

MAXIMUM
PRIN. STRESS

A	-2.000E+04
B	-1.500E+04
C	-1.000E+04
D	-5.000E+03
E	0.000E+00
F	5.000E+03
G	1.000E+04
H	1.500E+04
I	2.000E+04
J	2.500E+04
K	3.000E+04
L	3.500E+04
M	4.000E+04
N	4.500E+04

Enlarged View

Overall
Specimen

Figure IV.4: GIFTS Analysis of Stress Concentration at Hole

33

Stresses are first values
in boxes (psi) at orient-
ations shown.
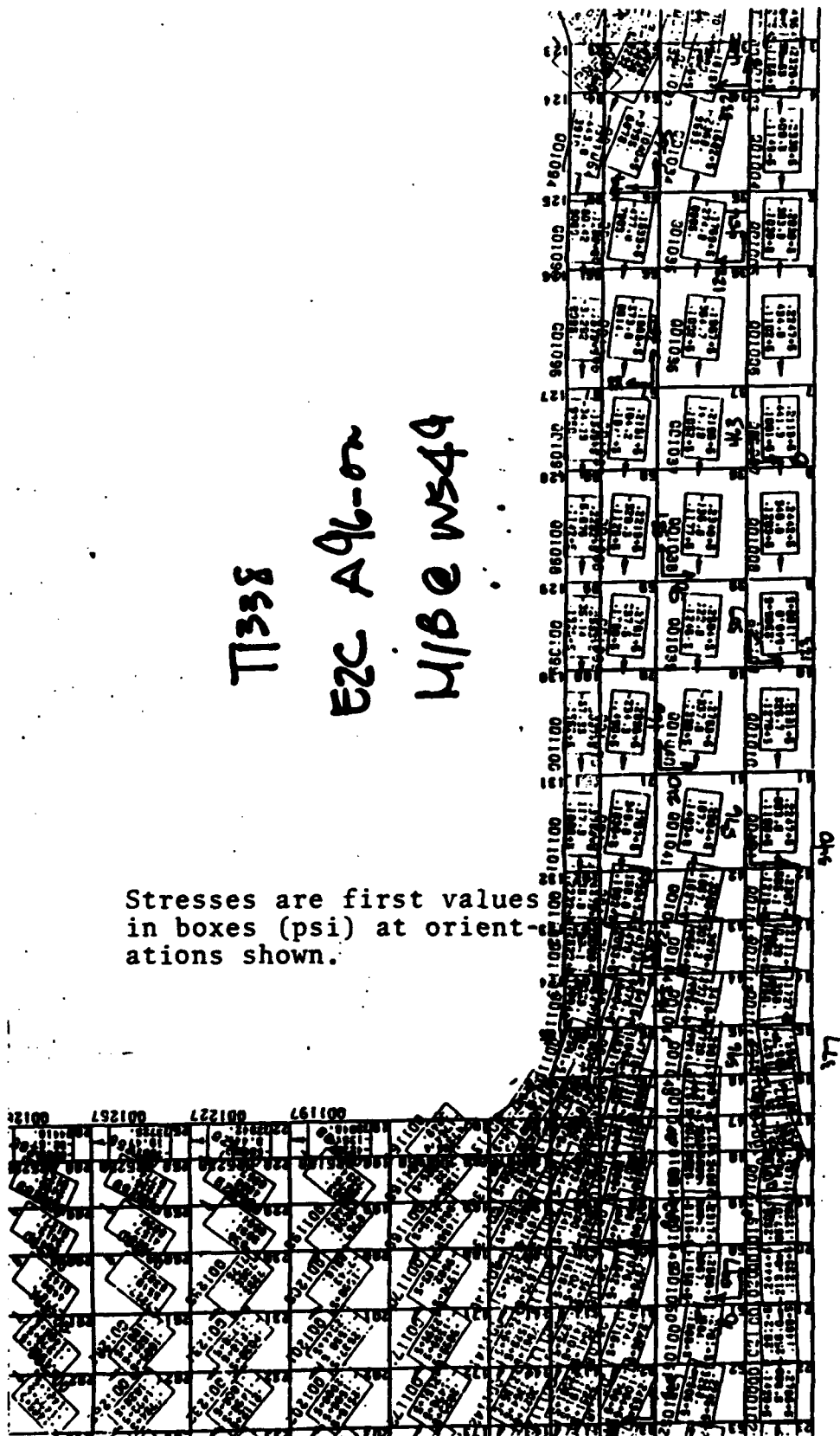
Figure IV.5: Grumman's Finite-element Model of Stresses

Stresses at
strain gauge
(kpsi)

Strain gauge locations

Figure IV.6:   Stress Readings from the Full-scale Fatigue Article
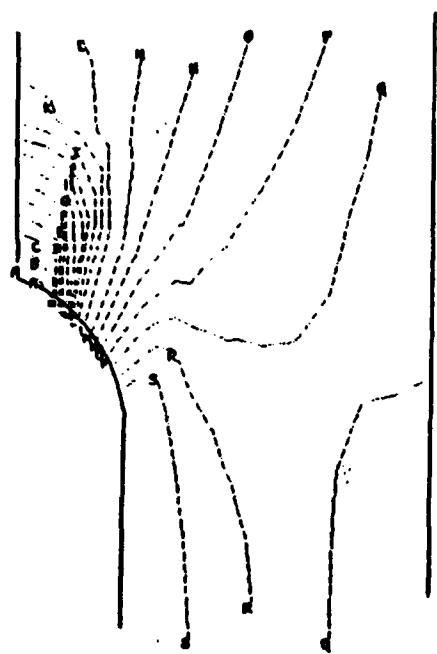
(a) Narrow slot
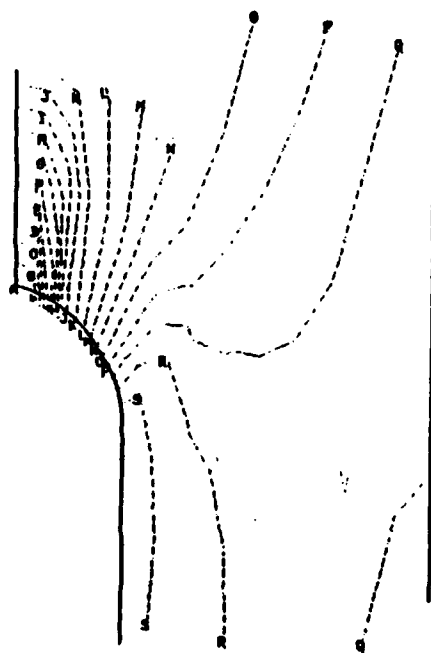
(b) Intermediate slot
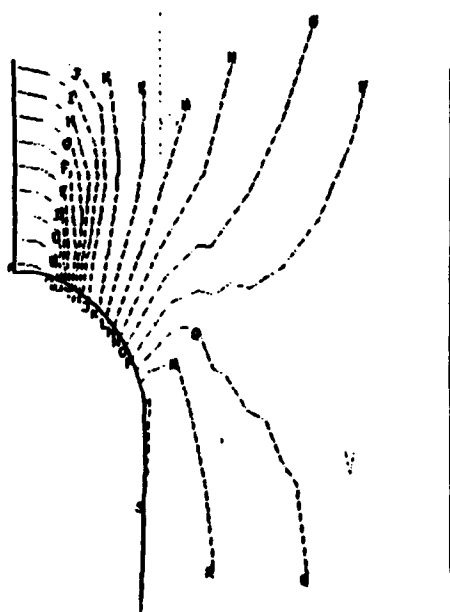
(c) Wide slot

PRIN. STRESS	
A	-1.000E+04
B	-7.500E+03
C	-5.000E+03
D	-2.500E+03
E	0.000E+00
F	2.500E+03
G	5.000E+03
H	7.500E+03
I	1.000E+04
J	1.250E+04
K	1.500E+04
L	1.750E+04
M	2.000E+04
N	2.250E+04
O	2.500E+04
P	2.750E+04
Q	3.000E+04
R	3.250E+04
S	3.500E+04

(d) Stress contour values (psi)

Figure IV.7: Effect of Widening Specimen Slot

36

aluminum sheet and in the longitudinal direction to minimize any residual rolling stresses in the sheet. Edges of the specimens were milled 0.125" to remove any shear stresses caused by cutting. A provision was included to bond aluminum tabs on the ends of the specimens using high shear strength epoxy (3M brand DP-110). This would have provided an additional sound-damping interface to reduce extraneous grip or machine noise but, after preliminary testing, it was decided that the tabs were unnecessary.

The fatigue spectrum for the aircraft was provided by Grumman. It was based on their analysis of statistical data on types of missions flown and accelerometer readings from the aircraft. This provided a block of 500 experimental flight hours (EFH), which contained 12,493 load cycles. Of these, only 6,818 cycles were identified as dynamic landing loads, which cause approximately 90% of the fatigue damage. These were the cycles that were used. Each cycle consisted of a pair of loads, corresponding to the maximum and minimum load at that flight condition. These loads were expressed as a percent of the average flight loading, or reference load. The stress level corresponding to this reference loading for the area of interest was 37,500 psi. Using minimum net cross-sectional area, the reference loading for the specimen was 13,209 lb. Each load percentage was multiplied by this reference load to generate a fatigue loading file which contained 13,636 loads (6,818 load pairs).

C.   MECHANICAL TESTING EQUIPMENT

An MTS Model 810 closed-loop, servo-hydraulic testing machine was specially modified for use in this test. Modifications to the load frame included remote mounting of the servo valve manifold, to isolate the frame from hydraulic switching and dither noise, and installation of a higher capacity servovalve to allow higher fatigue testing frequencies. The load cell and all transducer conditioners were checked and recalibrated prior to commencing testing. The maximum load capacity of both the actuator and the load cell was 100,000 pounds, divisible into four ranges of 10%, 20%, 50% and 100%. The actuator stroke position and load cell output were given as 0 to 10 V analog signals. This corresponded to a range in the parameter from zero to the maximum percent selected.

A constant stroke rate of 0.005" per minute was used for static testing. This provided a crack growth rate slow enough to avoid overloading the data gathering equipment, yet sufficient to complete the test in a reasonable amount of time (i.e. one half hour). Controller ranges selected were: 1" maximum actuator stroke (20% setting), 50,000 lb maximum load cell reading (50% setting), and 0.15 in/in maximum strain. This was the 100% setting for strain. Strain readings were taken only for the static tests using an MTS Model 632.11B-20 extensometer.

The controller ranges selected for the fatigue tests were 1" maximum actuator stroke (20% setting) and 20,000 lb maximum load cell reading (20% setting). The extensometer from the static test

38

was not used for the fatigue testing due to the added noise it caused by vibrating during fatigue. Also, strain readings were not directly transferable to stress values in the complicated stress field. For both the static and fatigue loading tests the specimens were placed in the test machine with no preloading and all outputs (actuator stroke, load cell and, if used, extensometer strain) zeroed.

An 8086 based, personal computer (Measurements Group Model 4125) was programmed to supply the loading spectrum to the MTS controller. The computer, which was equipped with a digital-to-analog (D/A) board (Metrabyte DAS-16G), supplied a digital word representing the desired load to the D/A board. The D/A board converted this digital word to an analog voltage in the range of 0 to 10 V. This voltage was proportional to the desired load and was fed into the MTS controller. The controller compared this command load with the load cell output and developed a voltage difference signal. This difference signal was then used to alter the specimen load to match the command load.

The computer itself was programmed in compiled BASIC. The program was designed to read each load value from the spectrum file and incrementally step up or down from its previous load value. This allowed a smooth and quiet transition between loads. The program then paused at the new load value and monitored the load cell output. When the load had been attained to within 5% or the number of monitoring attempts exceeded 6 tries, it proceeded to the next value in the cycle. This insured that the specimen reached

39

each load value, yet avoided having the program get 'hung up' in a loop during low loads where the voltage error in the load cell was greater than 5% of the total value. The process continued until all 13,636 of the load values in the spectrum block had been tested, at which point the program started again at the beginning of the block. It was found that the program could drive the testing machine smoothly and with minimal noise at a fatigue loading rate of better than 5 Hz.

To hold the specimen, a pair of grips were constructed in the Aeronautical Engineering machine shop. These grasped the specimen using sliding jaws that were clamped in place and held the specimen by friction. Unfortunately, the amount of force available by fully tightening the clamps was not sufficient to eliminate all slipping noise at the grips. However, this did provide an excellent opportunity to study this extraneous noise and differentiate it from actual crack noise.

D. ACOUSTIC EMISSION INSTRUMENTATION

To monitor the acoustic emission produced during the test, 5 Mhz broadband piezoelectric transducers (0.25" diameter Harisonic G0504) were used to capture the acoustic emission waves. An acoustic emission analyzer (Acoustic Emission Technologies 5500B system) was used to record certain waveform parameters (to be discussed below), while a digital storage oscilloscope (DSO) (LeCroy 9400A) was used to capture the entire waveforms.

1. Transducers

The piezoelectric transducers used were sensitive to the normal component of the surface displacement caused by a traveling stress wave. These particular transducers were chosen because of their reasonably flat response to frequencies in the region below 1 Mhz. This was extremely important in order to accurately measure the frequencies in the stress wave. The use of this type of broadband transducer is a break with tradition. In most previous studies, resonant transducers have been used to monitor AE due to their increased sensitivity. However, because of the frequency distortion at resonance the waveforms themselves were not studied. Accurate reproduction of the frequencies present provides a better means to understand the waveforms as well as the potential for more information [Ref. 22].

The transducers were attached to the specimen at the locations shown in Figure IV.8 using Dow Corning high vacuum grease as an acoustic couplant and bound in place using several wrappings of electrical tape. These locations were chosen in order to best detect acoustic emission from the expected crack growth between the hole and the cutout. Shown are the spacings from one transducer to another (in inches) and the distance from the transducer to the attachment hole and other transducers (in millimeters) (this later measurement was used by the AE analyzer as a 'yardstick' to locate events). Signals from the three transducers were input into the AE analyzer on channels 1, 2 and 4 (due to channel 3 being inoperative). Transducers 1 and 4 were positioned near the ends of

41
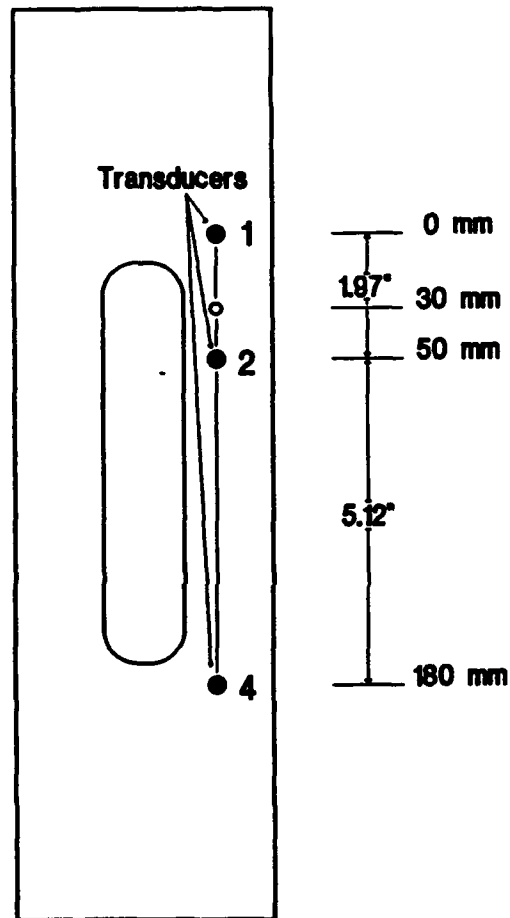
Figure IV.8:   Transducer Attachment Points

the specimen for use as 'guard' sensors. In this location they would be the first transducers triggered by a wave arriving through the grips (extraneous noise). This arrangement would permit spatial filtering. Transducer 2 was located as close as possible to the attachment hole (the assumed source of crack initiation), without blocking the view of the video microscope. Inputs from transducer 2 and transducer 4 were chosen for display on the DSO. Transducer 2 was chosen because it would be the first transducer triggered from an event at the hole. Transducer 4 was chosen due to its maximum distance from the hole and hence would show maximum separation between the extensional and flexural waveforms from events originating near the hole. This allowed the two waveforms to be distinguished by time of arrival. Recall that the reason the waves separate is due to the flexural waves slower speed.

2.   **AE Analyzer**

The AE analyzer was used to record the waveform parameters and provide linear location of AE sources. It consisted of several components. Preamplifiers were used to amplify and filter the signal from the transducers. A mainframe unit further amplified the signals, detected AE events, measured selected waveform parameters of those events, and computed the locations of the sources of the events. Finally, a stand alone personal computer was used to record events that were passed to it by the mainframe. The analyzer had the capability to handle up to eight channels of AE data and three channels of associated analog data. For this experiment only three AE and two analog channels were used

43

(corresponding to the three transducers and load cell and actuator stroke data).

Incoming signals from the transducers were first amplified by 60 db preamplifiers (AET Model 160B). A bandpass filter of 0.125 to 1.0 Mhz was incorporated and chosen primarily to screen out the lower frequencies associated with extraneous machine noise. From the preamplifiers, the signals traveled into the analyzer mainframe on one of the channels for the signal processing units (SPUs). The SPUs provided further, variable gain from 0 to 40 db, allowing a total gain of 60 to 100 db per channel. The amplified signals were compared against a preselected threshold voltage. Those exceeding the threshold caused an event· to be declared and were then passed on to a series of modules. These modules calculated event ringdown counts, event duration, rise time, peak amplitude and time difference of event arrival between the channels monitored. The time difference information was then used to compute the location of the AE source, based on previously supplied transducer position and wave speed data. This provided the opportunity for spatial discrimination of noise by eliminating those events from sources located outside the area of interest. Time based data (event duration, rise time and time difference of arrival) was measured using variable clock periods (125, 250, 500 or 1000 ns) to allow maximum accuracy for each datum. The entire process was coordinated by a computer (Computer Automation LSI 4/10 microprocessor with 32K RAM memory). Waveform parameters from the events were then passed (via a pico processor) to the parallel

communication bus of a personal computer (Wyse Model 3126). This PC was a 16 Mhz, 80386 based computer equipped with an 80387 math coprocessor chip, 3.712 megabytes of RAM and a 40 Mb hard drive. The computer stored the waveform parameters in real time, and also allowed display of the data in statistical or graphic form on either the video screen or through an attached printer. Postprocessing of the data was available, using any of the recorded waveform parameters to selectively filter the raw data.

During testing, the AE analyzer was set up to perform linear location as explained in Section III.C using the separation between the transducers. Clock periods for the rise time, event duration and linear locator (Δt) were all set initially to 125 ns (the minimum possible) in order to provide maximum timing accuracy for the expected short burst (dispersionless), extensional waves. The gain on the AE analyzer was set initially at 59 Db (just above ambient noise) for all channels monitored. The threshold level was set at 1.0 V (fixed), corresponding to the analyzer's default value.

3.   Digital Storage Oscilloscope (DSO)

The amplified waveform was fed into the DSO by an 'event-out' connection on the AE analyzer's SPU. The DSO was capable of digitizing and storing 32 Kb of data on two separate channels simultaneously. A sampling rate of 50 megasamples per second was used in these experiments. The recorded data was passed to a PC (Compaq Deskpro Model 386/20) via a GPIB board. The PC was a 20 Mhz, 80386 based computer equipped with an 80387 math coprocessor

chip, 2.048 Mb of RAM and a 60 Mb hard drive. The typical turnaround time between triggering of the DSO, waveform storage and trigger reset was approximately 2 seconds. The total storage capacity of the PC was about 1120 waveforms. Postprocessing of the data allowed the recall of any of the waveforms stored on the computer. The DSO also incorporated built-in Fast Fourier Transform (FFT) firmware to allow frequency analysis of the waveforms. The waveforms could be plotted (with an HP-7470A Plotter) by using the RS-232-C plotter port on the DSO.

During testing, the DSO was set to capture waveforms automatically, with a time division of 50 μs/division (500 μs total) and voltage division of 2 V/division (16 V total peak-to-peak) at 50 Ω input impedance (matched with the AE analyzer output).

4. Calibration

Calibration runs for the AE analyzer's linear locator and the DSO were performed using lead breaks. The use of lead breaks involves breaking a certain type of mechanical pencil lead (Pentel 2H, 0.5 mm) to create an acoustic emission source very similar to the standard, glass capillary source used at the National Institute of Standards and Technology. The original concept was proposed by Hsu and Hardy [Ref. 26] and later refined by the National Institute of Standards. The use of lead breaks to create extensional and flexural waves in aluminum has been shown by Gorman [Ref. 22]. To analyze the lead breaks a Fast Fourier Transform was performed on both extensional and flexural waveforms, using the built-in

46

firmware of the DSO. The FFT was computed using 2500 data points, with an effective sampling frequency of 2.5 MHz. The results were displayed as a Power Spectrum (dB vs. Hz). The DSO plots of these calibration runs were typical of those obtained throughout the investigation and are shown in Figure IV.9. Each plot shows the original signal on the center line (voltage vs time). At the bottom of each plot is shown the frequency distribution (dB vs KHz). The extensional wave (a) is seen to contain higher frequency components than the flexural wave(b). These calibration runs confirmed the ability to linearly locate the source of an event using the AE analyzer and the ability to discriminate between extensional and flexural waves captured by the DSO.

The use of the time difference of arrival at different transducers verified that the transducers were receiving the same wave and not a reflection. The speed of the extensional wave in this aluminum plate was calculated to be 208,000 in/sec and the flexural wave as 114,500 in/sec at 400 KHz (approximately the highest flexural wave frequency observed and hence, according to equation (31) in Section III.A, the fastest component). The straight line spacing between transducers 2 and 4 (5.12") should therefore have produced a time delay of 24.6 μs for the extensional wave. This delay correlated closely with the observed Δt and waveform data. Plots of the waveform produced by a lead break inside the hole are shown in Figure IV.10. Here the difference between the time of arrival of the extensional wave at transducer 2 (a) and transducer 4 (b) was 28 μs.

(a) Extensional wave

(b) Flexural wave
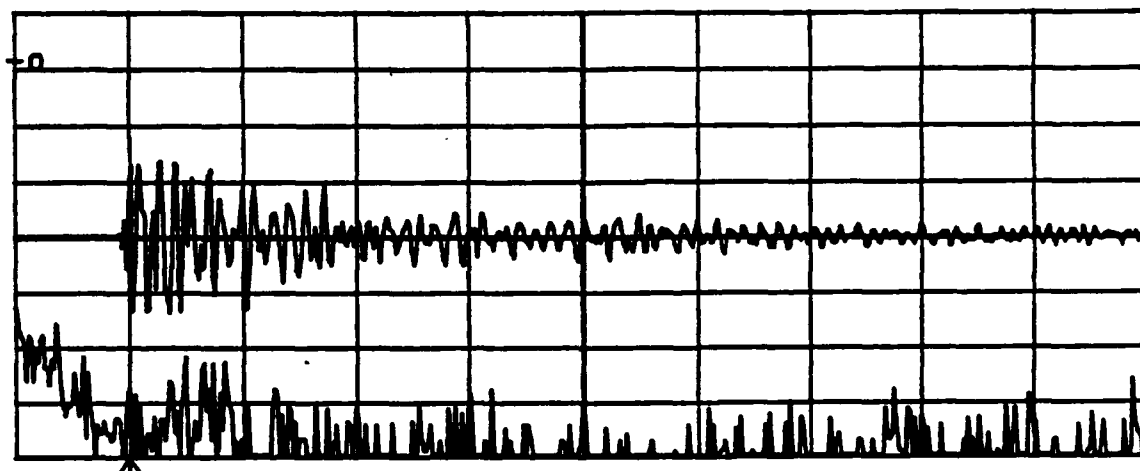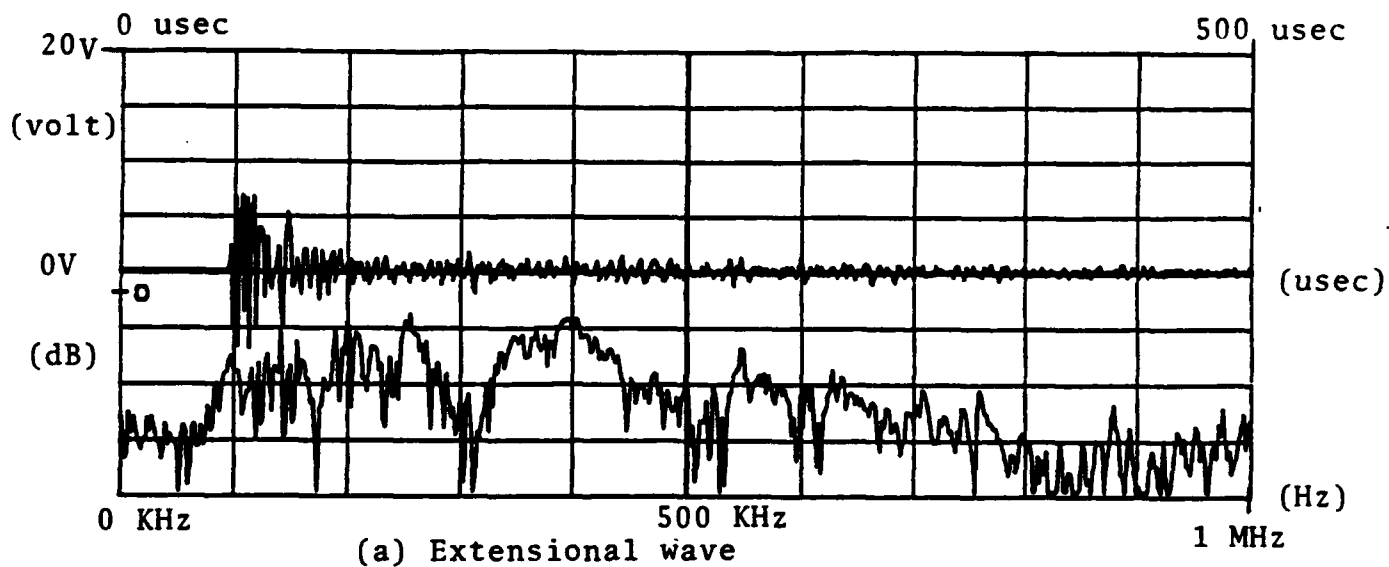
Figure IV.9: DSO Plots of Lead Breaks

(a) Transducer 2

0 usec ▲ t=28usec 500 usec

(V)

(dB)

0 KHz 500 KHz 1 MHz

(b) Transducer 4
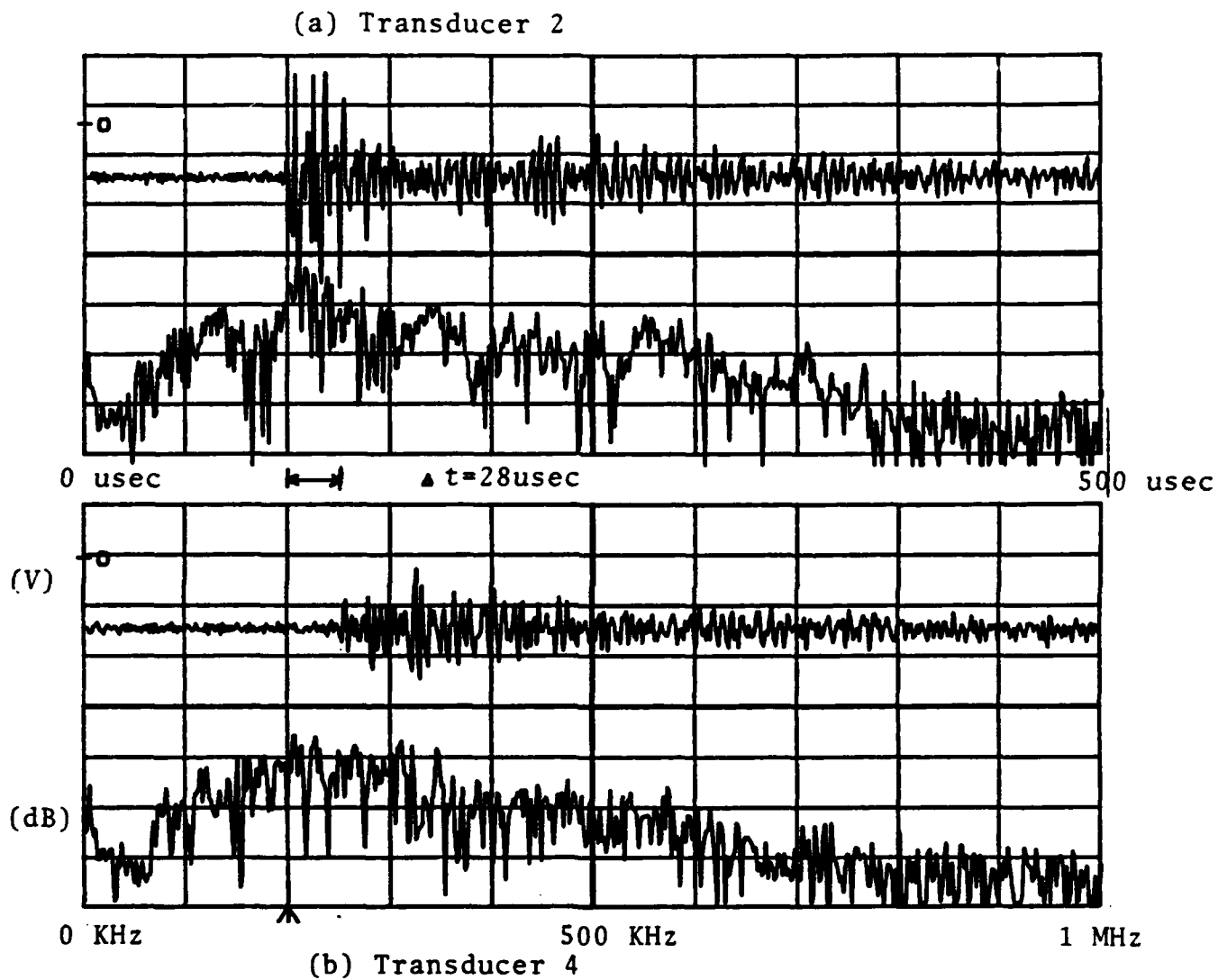
Figure IV.10: Measurement of Time of Arrival Using DSO

49

Following successful calibration the waveforms created by both crack events and extraneous noise were simulated. An in-plane lead break in the hole was used to simulate the crack events. To simulate the noise created by grip slippage or crack face rubbing, an aluminum tab was scraped across the specimen. Both waveforms were recorded and compared using FFTs of the signals. The simulated crack consisted of both the extensional and flexural modes, although the flexural wave was heavily filtered. The portion of the signal seen in Figure IV.11 (b) immmediately after the extensional wave is due to the many reflections, which are a result of the narrow specimen geometry. It is clear from the figure that the wave created by a lead break (b) has higher frequency components present than the wave created by friction (a). Based on the above calibration and simulations, it was determined that a reliable test for discriminating between noise and crack waveforms was available.

E.   VIDEO MICROSCOPY

The primary means used to verify crack growth in the specimen during testing was video microscopy. The system was composed of several components: a video camera and high-power lens, a high resolution monitor and electronic double-reticle, a time lapse video cassette recorder (VCR), and a video hard copy unit. The system was not available during static testing so a 70x binocular microscope was temporarily used to visually monitor the area of interest.
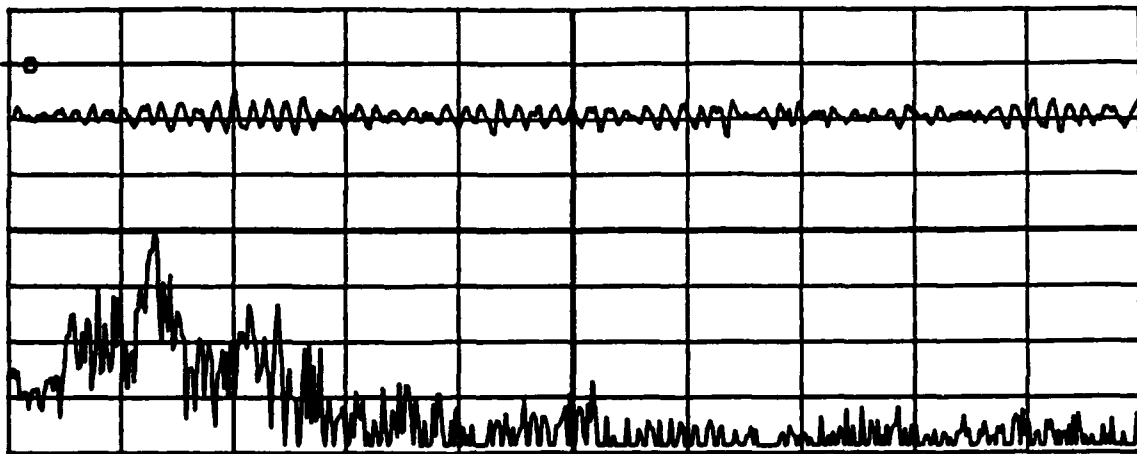
(a) Signal created by scraping a piece of
aluminum on a specimen

(b) Extensional wave created by a lead break
in the attachment hole
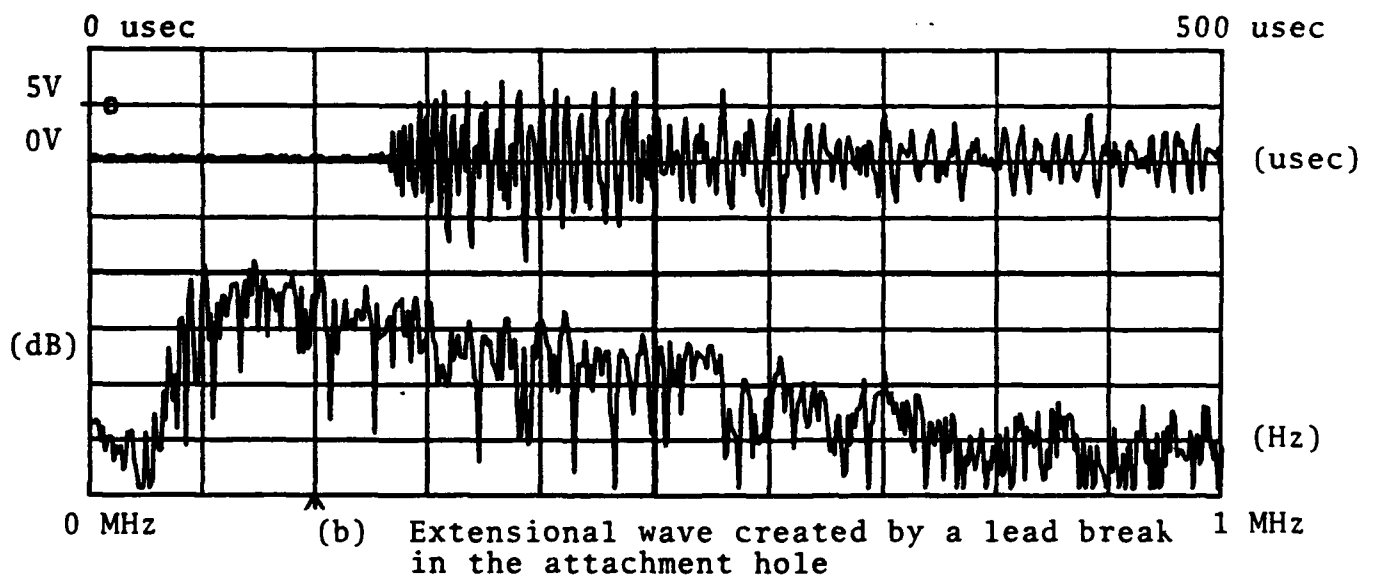
Figure IV.11: Comparison between Simulated Noise
and Simulated Crack

The camera used was a 0.5" charged circuit device (CCD) black-and-white video camera (Micro-Mac V-A). It was capable of 450 line horizontal resolution using a 610x488 (horizontal x vertical) pixel matrix. A zoom lens with a magnification range from 64x to 400x (when used with a 12" monitor) was attached to it. A combination of light sources (fluorescent and incandescent) were used to provide optimal lighting for the test. The camera and lens were mounted on an x-y-z (left/right, up/down and focus in/out) camera mount, capable of remotely controlled, fine adjustment scanning in 0.002" increments.

The video output from the camera was routed to a time lapse VCR for recording. The VCR (Panasonic Model AG-6720A-P) used a Super VHS recording format for 400 line resolution at all speeds. The time lapse mode was obtained by varying the amount of time between frames recorded (rather than varying the tape speed) for a variety of maximum recording times. The 24-hour mode was used in the fatigue portion of this test, while tests involving crack growth were recorded at full-speed (2-hour mode). The VCR also contained circuitry specifically designed for frame-by-frame viewing, which was necessary for a clear picture when the tape was paused to measure crack length. A superimposed, elapsed time indicator was used to correlate AE events from the AE analyzer with the observed crack growth.

A 12" black-and-white monitor (Javelin Model BWM12) was used to observe the testing. The monitor had an 800 line horizontal resolution. A video hard copy unit (Mitsubishi P-60U) was used to

provide copies of the images observed. The unit used thermal heads to provide a 16 tone, gray scaled image with 400 line resolution using a 640x476 pixel matrix. Finally, an electronic double-reticle generator (Techni-Quip Model T-Q/DA) provided the means to superimpose two cross-hairs on the image for measuring crack sizes at known magnifications.

The assembled video microscopy unit was focused on the specimen using 70x magnification (maximum field of view) to observe the innermost radius of the hole facing the slotted cutout. This corresponded to the region of maximum stress from earlier calculations and the area that the crack was expected to originate from. By combining together the minimum resolutions of the components, it was found that the smallest crack sizes theoretically measurable were on the order of 0.001" at 400x magnification.

V. RESULTS

A. STATIC TESTING

Quasi-static, monotonically increasing displacement-to-failure tests on the specimen were used to verify the AE detection capabilities of the equipment and to detect crack initiation in a low-noise environment. A total of three static, ramp-to-failure tests were performed on specimens S1, S2, and S3 respectively.

The first test showed, as expected, that the majority of the acoustic emission was composed of extraneous noise, as determined by its order of arrival at the transducers. This noise appeared to be characterized by waves of varying amplitudes. Each was identified by performing an FFT on the waveform and noting the lack of high frequency components above 200 Khz. The amplifier gain had to be adjusted several times in order to find a threshold above the level of this noise. As the load on specimen S1 (23,949 lb) approached yield stress (73,000 psi), a number of extensional waveforms were observed. The source of these events was located by the AE analyzer to be in the vicinity of the hole-cutout interface, the average value within 0.04" of the actual crack. The DSO plots of both waveforms and their FFTs are shown in Figure V.1(a) and (b) respectively. These clearly show that the noise signals do not contain the higher frequency components seen in the probable cracking. These higher frequency components are associated with extensional waves. Further, the time difference of arrival between transducers 2 and 4 correlated to a wave traveling at the speed of
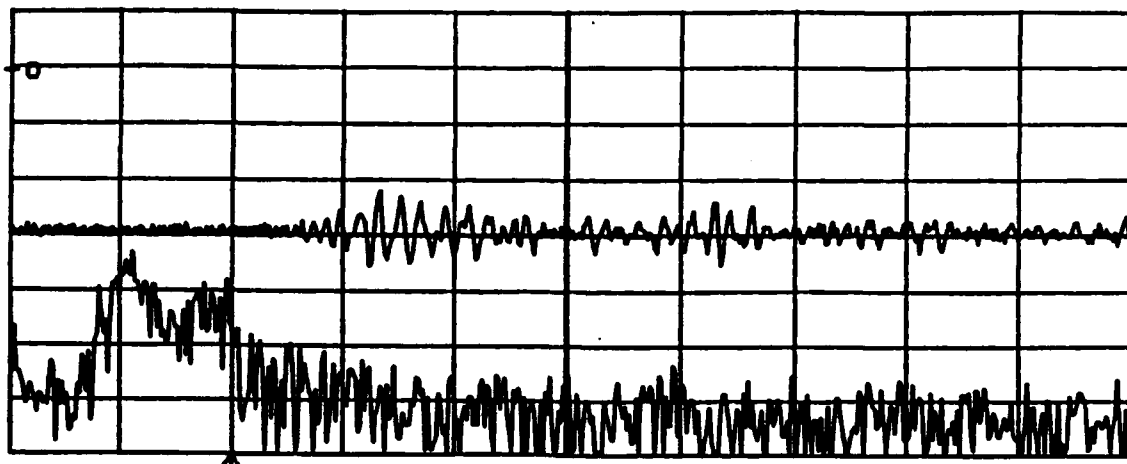
(a) Extraneous noise
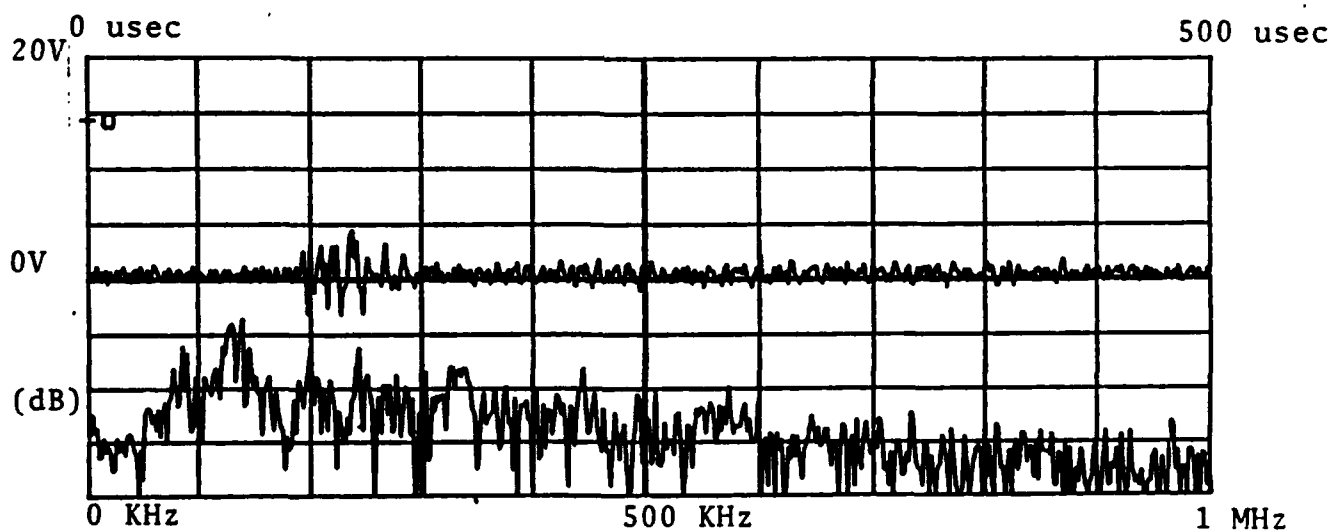
(b) Crack events - extensional waveform

Figure V.1: Comparison of Observed Flexural and Extensional Waves

55

the extensional wave. This method of characterization is believed to be a new and practical tool for distinguishing waveforms and classifying noise from crack initiation and growth.

The AE events continued to occur until the specimen failed by 'necking' at 25,000 lb. Failure occurred as expected (based on the finite-element model's region of maximum stress) between the hole and the curved section of the cutout slot. Observations of the crack face showed primarily ductile failure with the surface oriented in a 'V' shape corresponding to shear failure. Also, it should be noted that, while this was the region of highest predicted stress concentration, it was also the region of minimum cross sectional area. This proved to be significant under static loading, since stress concentration factors predicted a much lower failure loading. Instead, the net section was the dominant factor in failure. The results also showed that some of the AE analyzer's event duration and linear locator counters had overflowed with events exceeding the maximum timing period. Clock periods for these parameters therefore had to be increased. This increased the maximum observable time period at the expense of decreased accuracy in event duration timing and linear location. Finally, it was discovered that the AE analyzer's power supply was faulty and had injected extraneous noise into the system by shorting across some of the transducer inputs. Replacing the power supply allowed the system gain to be increased for the remaining tests.

The second test was run at a system gain of 100 dB (maximum) and AE analyzer clock periods of 500 ns for both the event duration

and linear locator modules. All other settings remained the same as in the first test. Failure of this specimen (S2) occurred at 23,450 lb, in a manner nearly identical to S1. Several significant results were obtained. First, the onset of extensional waveforms, again determined by the AE analyzer as coming from the region surrounding the hole, now occurred prior to overall yield stress. The AE instrumentation was now detecting the crack initiation phase earlier in the stress region surrounding the hole due to the increased system gain. Secondly, the crack events were observed to occur in 'packets', that is, several crack events occurring sequentially in rapid succession. This sequence of events due to crack extension differed from the events due to extraneous noise, which appeared to occur randomly. It was believed that what was being observed was actual crack growth in the form of AE events due to microfracture of the intermetallic inclusions. Later, during fatigue testing, it was often possible to identify crack growth by locating these groupings of events on the AE analyzer's parametric printout and correlating them with an extensional waveform from one of these events on the DSO. It was not possible to do this for the static case, however, due to the short amount of time between onset of cracking and final failure (approximately 20 seconds).

The third and final static test with specimen S3 proceeded in the same manner as the second, except that the system gain was reduced to 90 dB. This was done in order to reduce the size (peak-to-peak voltage) of the extensional waves observed just prior to failure. These events, observed with specimen S2, were of such a

large amplitude that they overloaded the input at the DSO. Further analysis of the data indicated that the smallest observed peak amplitude of the crack events was approximately 50 dB. This correlated to 3.16 V. At 100 dB, a 3.16 V amplifier output correlates to a 31.62 μV event at the sensor. This same event yields a 1.00 V amplifier output when amplified by 90 dB. Thus 90 dB was chosen as approximately the proper gain for the fatigue measurements. Further, the 1 MΩ input impedance was selected on the DSO, which doubled the measured voltage at the DSO due to impedance mismatching yet allowed an increase to 5 V/division (40 V peak-to-peak). This allowed relatively larger amplitude waves to be captured without overloading the DSO. Results of the third test confirmed those of the second test. Extensional waves were again observed to occur below yield stress and were located in the vicinity of the hole-cutout interface. Thus, crack growth using linearly located, extensional waveforms was tentatively identified. Visual identification of the slower growth rate of the cracks during fatigue confirmed this identification.

B. FATIGUE TESTING

Three fatigue tests were run on specimens F1, F2, and F3 respectively. For the first fatigue test the AE instrumentation settings were the same as for the last static test. The system had a lower level of extraneous noise than expected so the system gain was set to 95 dB initially. However, during the testing of specimen F1, the amount of extraneous noise was observed to

increase, as evidenced by order of arrival at the transducers. This noise was probably caused by the specimen slipping in the grips. The test was paused twice to tighten the specimen grips and the amount of system gain gradually reduced to 60 dB (the minimum possible with 60 dB preamplifiers). This reduction in gain was necessary to avoid excessive triggering of the DSO and consequent overloading of the DSO computer's waveform storage space. This also allowed sufficient turnaround time between waves to capture and store each one. (It should be noted that a better arrangement for specimen fixturing would probably have alleviated most of this noise. However, as will be seen, the waveforms due to cracking were easily separable from those due to noise.) The specimen fractured completely after more than 21 hours of testing. This was at approximately 403,200 cycles (14,800 EFH). Observation of the crack face showed unmistakable evidence of the 'beach-marks' associated with fatigue failure. This is shown in Figure V.2. Cracking had occurred to a maximum depth of 0.135" on the inward side (a), and 0.068" on the outward side of the hole (b). Due to the concave shape of the crack face, the surface crack would have been smaller.

The AE results from this first test were limited, due to the lower than desired system gain at failure. However, certain data were available. Again it was noticed that extensional waveforms occurred in 'packets', which were thought to be AE events from the growing crack based on the observations discussed earlier (see Section V.A on Static Testing). This grouping of events occurred

59

0.135"
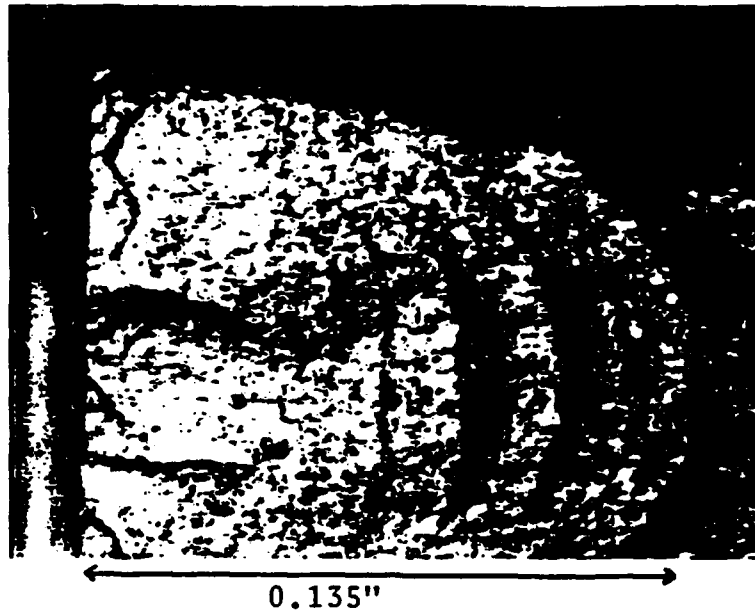
(a) Crack between hole and slot, 64x

0.068"

(b) Crack between hole and edge, 64x

Figure V.2: Fatigue Cracking on Specimen F1

during a single load cycle, indicating 'bursts' of crack growth. An example of this grouping on the AE analyzer's printout is shown in Figure V.3. Groups of events are shown in brackets. Extraneous noise, identified through linear location and characterized by low frequency content, usually occurred only once during a single load cycle. Unfortunately, all of the waveforms were not as distinct as those produced by lead breaks. It is possible that several waveforms were present, with components of both the flexural and extensional waves occurring at the same time as a result of multiple events interacting. It was here that the effectiveness of using FFTs to discriminate a non-recognizable waveform became apparent.

The second test using specimen F2 used settings identical to the first, except that the system gain was set to 70 dB until a surface crack of 0.024" in length was observed by video microscopy at approximately 397,700 cycles (14,600 EFH). As the results for the first fatigue test showed, the surface crack length was usually less than the total crack depth. The gain was then increased to 90 dB and the crack growth monitored until the crack reached 0.086" at approximately 409,300 cycles. At this point it was determined that sufficient data had been collected and the test was stopped. A visual record of the crack growth from the attachment hole towards the slot may be seen in Figure V.4. Post processing of the data revealed that crack initiation was detected by AE at approximately 392,700 cycles (14,400 EFH), when the first linearly located, extensional waveform was detected (the crack length at that time

TST SENS	RDC	ED	PA	ENG	RT	SLOPE	EVENT TIME	RG	LOC	PAR1	PAR2	PAR3
% 1*1	1	1	44	44	1	158	21:27:49.66			2520	0	160
% 1*14	5	46	46	63	6	33	21:27:50.62			3730	0	240
% 1*1	1	1	44	44	1	158	21:27:52.62			2580	0	170
# 1 21	4	19	53	66	3	149	21:27:52.77	2	35	2580	0	170
# 1 21	1	1	45	45	1	177	21:27:52.78	2	33	2580	0	170
% 1 214	1	1	46	46	1	251	21:27:52.79			2580	0	170
# 1 214	184	1477	76	108	121	52	21:27:52.79	2	45	2580	0	170
% 1 214	1	1	44	44	1	158	21:27:52.80			2580	0	170
# 1 124	4	20	48	61	7	36	21:27:52.81	2	23	2580	0	170
# 1 214	8	25	59	73	3	296	21:27:52.81	2	35	2580	0	170
% 1 214	1	1	42	42	1	126	21:27:52.82			2580	0	170
# 1 124	4095	65520	61	109	34	33	21:27:52.82	1	18	2580	0	170
# 1 214	4	15	51	63	1	354	21:27:52.84	2	33	2580	0	170
# 1 214	7	24	55	69	6	94	21:27:52.84	2	35	2580	0	170
# 1 214	178	1513	77	109	3	2354	21:27:52.85	2	33	2580	0	170
% 1 214	4	10	47	57	6	37	21:27:52.85			2580	0	170
# 1 214	2	8	51	60	1	354	21:27:52.87	2	38	2580	0	170
% 1 21	4	16	51	63	1	354	21:27:52.88			2580	0	170
# 1 21	8	24	52	66	6	66	21:27:52.89	2	33	2580	0	170
% 1*2	1	1	42	42	1	126	21:27:52.93			2580	0	170
# 1 214	6	24	58	72	3	264	21:27:52.94	2	33	2580	0	170
% 1 124	11	308	48	73	5	50	21:27:52.95			2580	0	170
# 1 21	3	7	47	55	1	223	21:27:52.96	2	40	2580	0	170
% 1*2	1	1	45	45	1	177	21:27:52.97			2580	0	170
# 1 214	11	118	63	64	3	470	21:27:53.00	2	35	2580	0	170
% 1*2	1	1	40	40	1	100	21:27:53.03			2580	0	170
# 1 21	5	18	52	65	3	132	21:27:53.06	2	33	2580	0	170
% 1 124	20	247	51	75	6	59	21:27:59.10			4900	0	300
% 1 124	24	282	51	76	17	21	21:28:52.13			3430	0	210
% 1 12	2	5	49	56	1	281	21:28:56.33			4050	0	260
% 1*1	1	1	42	42	15	8	21:28:58.18			2580	0	180
% 1*1	1	1	39	39	1	89	21:28:59.64			2730	0	180
% 1 12	1	1	41	41	1	112	21:29:00.23			2730	0	180
% 1*1	1	1	45	45	1	177	21:29:02.25			2730	0	180
# 1 12	1	1	44	44	1	158	21:29:02.34	1	18	2730	0	210
# 1 21	6	23	52	66	1	397	21:29:06.32	2	45	3060	0	210
% 1*2	2	4	47	53	3	74	21:29:06.34			3060	0	210
% 1*1	1	1	44	44	1	158	21:29:09.41			6510	0	390
% 1*14	5	91	44	64	1	158	21:29:11.05			3270	0	210
% 1 12	11	86	46	65	40	5	21:29:14.00			2580	0	170
% 1 124	3	30	44	59	1	158	21:29:15.35			3800	0	240
% 1 124	21	188	49	72	22	13	21:29:19.87			2890	0	190
% 1*1	2	6	46	56	1	251	21:29:23.00			2570	0	150
# 1 124	8	93	47	67	9	25	21:29:24.67	1	10	4310	0	270
% 1*1	1	1	41	41	1	112	21:29:25.40			4310	0	270
% 1*142	2	22	44	57	1	158	21:29:26.11			2460	0	150
% 1 124	8	53	46	65	29	9	21:29:31.34			3770	0	230
# 1 214	6	33	57	72	3	235	21:29:34.40	2	33	2650	0	170
% 1*1	2	35	45	60	34	5	21:29:34.41			2650	0	170
% 1*2	5	19	51	64	2	177	21:29:34.42			2650	0	170
% 1*2	1	1	46	46	1	199	21:29:34.44			2650	0	170
% 1 214	1	1	43	43	1	141	21:29:34.45			2650	0	170
% 1 214	1	1	46	46	1	199	21:29:34.47			2650	0	170
# 1 214	4	13	51	62	3	118	21:29:34.50	2	33	6870	0	410
# 1 21	2	7	46	54	1	199	21:29:34.51	2	45	6870	0	410
# 1 21	1	1	49	49	1	281	21:29:34.54	2	43	6870	0	410
# 1 21	2	4	45	51	3	59	21:29:34.57	2	45	6870	0	410
% 1 12	2	5	45	52	1	177	21:29:35.57			4930	0	280
% 1 12	4	127	48	70	1	281	21:29:36.02			4930	0	280
% 1 124	13	129	57	78	4	177	21:29:36.83			4040	0	240
% 1 124	17	293	49	74	96	3	21:29:45.52			3250	0	210
% 1*14	10	114	44	65	46	3	21:31:37.93			3620	0	230
% 1*1	1	1	46	46	1	199	21:31:38.17			3620	0	230
% 1*1	1	1	42	42	1	126	21:31:40.63			3390	0	210
% 1*1	1	1	43	43	1	141	21:31:43.65			3360	0	220
% 1*1	2	9	44	54	1	158	21:31:44.68			5240	0	300
% 1 124	56	460	63	90	18	78	21:31:52.28			2860	0	190
% 1 124	5	39	46	62	6	33	21:32:00.74			2460	0	150
% 1*1	2	5	46	53	3	66	21:32:04.47			3950	0	250
% 1 124	11	246	46	70	12	17	21:32:06.07			3130	0	200
% 1*1	1	2	44	47	1	158	21:32:07.36			2650	0	180
# 1 21	3	11	46	56	4	50	21:32:07.48	2	35	2650	0	180
% 1 12	8	136	50	71	50	6	21:32:07.71			2650	0	180
# 1 214	4	13	56	67	3	210	21:32:07.74	2	33	2650	0	180
% 1 124	7	107	53	73	1	446	21:32:09.40			2090	0	150
% 1*1	1	1	40	40	50	2	21:32:16.13			2590	0	170

Figure V.3: Grouping of Events on AE Analyzer

(a) 0.028" crack-397,700 cycles
250x

(b) 0.053" crack-403,100 cycles
150x

(c) 0.086" crack-409,300 cycles
70x

Figure V.4:   Crack Growth in Specimen F2

could not be determined but was interpolated to be less than 0.01"). The waveforms and FFTs associated with noise, crack initiation and crack growth are shown in Figure V.5.

For the third fatigue test the system gain set initially at 75 dB. This test ran significantly longer than the first two. A crack of 0.018" was observed visually at approximately 636,700 cycles (23,300 EFH). The system gain was then increased to 95 dB and the crack growth monitored using both AE and visual means. The test was stopped at approximately 641,300 cycles, with a crack length of 0.025". Post processing revealed that crack initiation had not been detected acoustically at 75 dB, even though review of the video tape identified a 0.004" crack beginning at approximately 622,200 cycles (22,800 EFH). It was only after the system gain was increased to 95 dB that the AE analyzer began detecting the crack. The reason for the significant increase in fatigue life is not known.

To determine the minimum detectable crack length, a crack growth of 0.01" was monitored in specimen F3. The video microscope was focused on the crack at 250x magnification and the superimposed reticle was set for 0.01" beyond the initial crack tip. A dye penetrant was used to highlight the crack (Met-L-Chek VP-30, water soluble, visible dye). The accompanying developer coating was not used because it was found to obscure the crack at 250x. The system gain was set to 90 dB, with all other parameters as previously set. The fatigue loading spectrum was run at 2 Hz. This slower testing rate was used in order to more accurately distinguish between AE

20V

0V

(dB)

0 KHz   500 KHz   1 MHz
0 usec   500 usec

(a) Noise signal

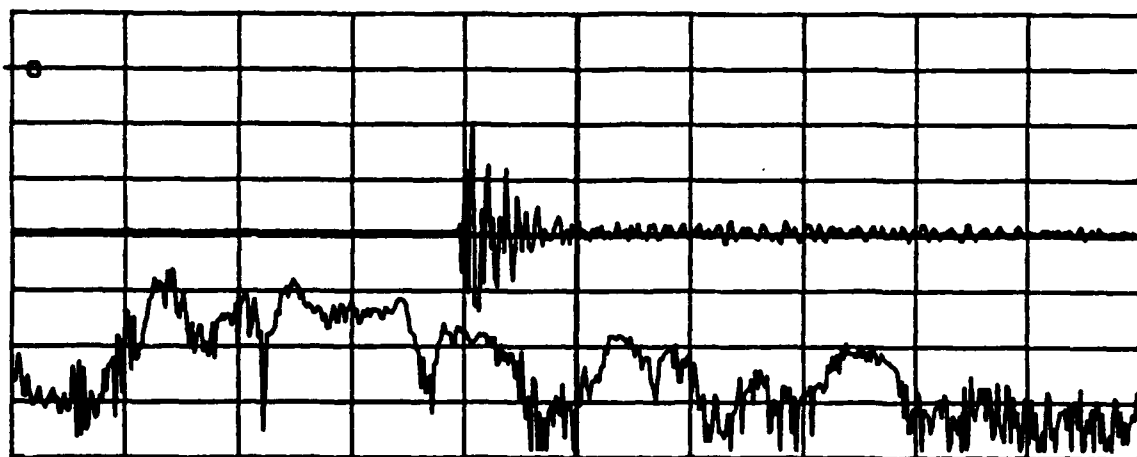(b) Crack initiation signal

(c) Crack growth signal
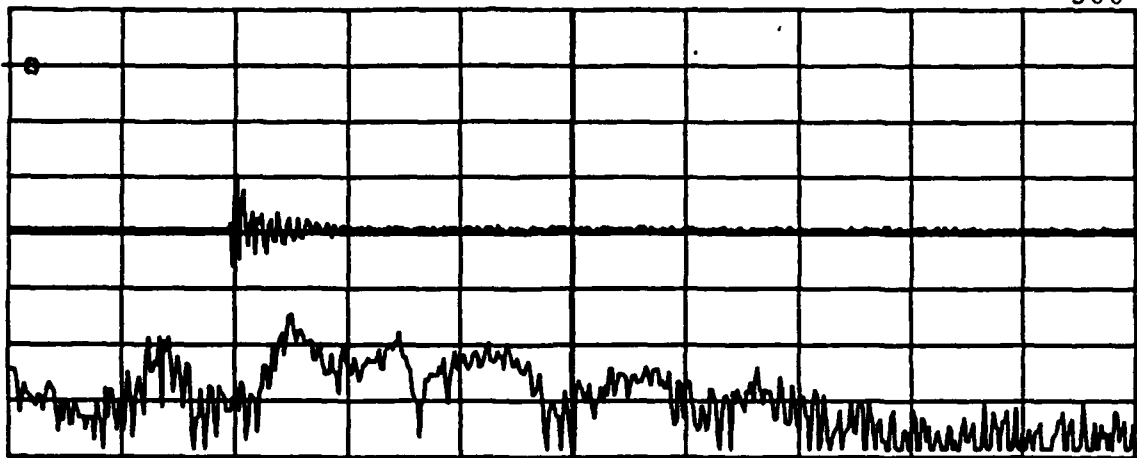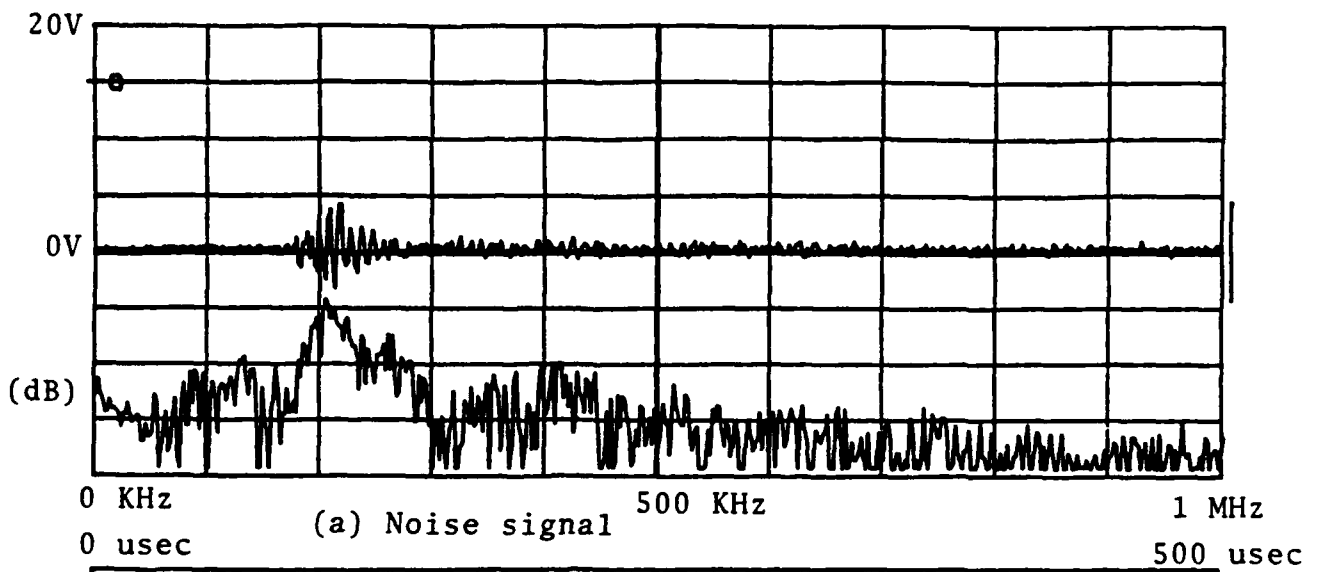
Figure V.5:   DSO plots of Noise, Crack Initiation and Crack Growth

65

events and to allow the DSO time to capture every waveform at the higher gain. A steady rate of valid (crack related, extensional waveforms) AE events was observed, accumulating a total of 16 events after approximately 9,200 cycles, during which time the crack had grown 0.008". The number of valid AE events then increased, so that 19 more events were recorded until after approximately 12,000 cycles total, when the crack length had grown a total of 0.010". Even though a faster fatigue rate would miss some of these events, it is believed that a crack initiation of 0.005" in length or smaller could be detected. This would require that the system be operating at a gain of 90 dB or better.

VI. CONCLUSIONS

A current problem with fatigue cracking in the E-2C Hawkeye has been modelled and monitored using acoustic emission. Previous work in acoustic emission has attempted to discriminate signals due to crack growth from those due to extraneous noise. However, this work has only examined certain parameters of the wave and not the waveform itself. Recent studies have shown that it is possible to discriminate among the two modes of stress waves in plates. The present work has built on this to provide a new method for discriminating crack growth signals. Specifically, it has:

- demonstrated experimentally that crack growth signals are in the form of extensional waves.

- shown experimentally that extraneous noise signals contain primarily lower frequency components (below 200KHz).

- discriminated between the two waveforms by using time difference of arrival and FFTs to check for the faster wavespeeds and high frequency components present in extensional waves.

- established a minimum detectable crack length of approximately 0.005" in 7075-T6 aluminum using a high system gain of 90 dB or greater.

Additional work could proceed to correlate the source of crack events by studying the fatigue crack face. A correspondence should exist between the number of broken intermetallic inclusions in the plastic zone surrounding the crack and the number of observed extensional AE events. This would establish the link between the observed crack growth waveform and its emission source. Due to the

67

complex nature of the plastic zone, this may be a very difficult task. However, from a practical point of view, knowledge of the true nature of the source of the emission may not be required.

Further study on a more complex specimen containing fasteners should verify the usefulness of this technique and its applicability to current problems with extending the life of aging aircraft.

LIST OF REFERENCES

1. Grumman Aerospace Corporation Report 3380.02, <u>Test Plan for Fatigue Test of E-2C Aircraft</u>, by R. Price, S. Campbell and T. Balderes, pg. 7, 30 June 1984.

2. Grumman Aerospace Corporation Report AV123-U-RP-292, <u>E-2C Fatigue Test Wing Center Section Teardown Inspection Report</u>, by P. Moll and J.Savalli, pg. 1.0.1, 21 November, 1989.

3. Gerberich, W.W. and Hartblower, C.E., "Some Observations on Stress Wave Emission as a Measure of Crack Growth," <u>International Journal of Fracture Mechanics</u>, Vol. 3, No. 3, pp. 185-191, September 1967.

4. Gillis, P.P., "Dislocation Mechanisms as Possible Sources of Acoustic Emission," <u>Materials Research and Testing Standards</u>, Vol. 11, No. 3, pp. 11-13, March 1971.

5. Tetelman, A.S, "Acoustic Emission Testing and Microfracture Processes," <u>Materials Research and Testing Standards</u>, Vol. 11, No. 3, pp. 13-16, March 1971.

6. McBride, S.L., Maclachlan, J.W., and Paradis, B.P., "Acoustic Emission and Inclusion Fracture in 7075 Aluminum Alloys," <u>Journal of Nondestructive Evaluation</u>, Vol. 2, No. 1, pp. 35-41, January 1981.

7. Smith, S. and Morton, T.M., "Acoustic-emission Detection Techniques for High-cycle-fatigue Testing," <u>Experimental Mechanics</u>, Vol. 13, No. 5, pp. 193-198, May 1973.

8. Harris, D.O., and Dunegan, H.L., "Continuous Monitoring of Fatigue-crack Growth by Acoustic-emission Techniques," <u>Experimental Mechanics</u>, Vol. 14, No. 2, pp. 71-81, February 1974.

9. Morton, T.M., Harrington, R.M., and Bjeletich, J.G., "Acoustic Emissions of Fatigue Crack Growth", <u>Engineering Fracture Mechanics</u>, Vol. 5, No. 3, pp. 691-697, September 1973.

10. Morton, T.M., Smith, S., and Harrington, R.M., "Effect of Loading Variables on the Acoustic Emissions of Fatigue-crack Growth," <u>Experimental Mechanics</u>, Vol. 14, No. 5, pp. 208-213, May 1974.

11. Singh, J.J, and Davis, W.T., "Evaluation of Acoustic Emission Technique for Crack Growth Measurement in Aeronautical Structures," 20th International Instrumentation Symposium, Albuquerque, New Mexico, Instrument Society of America, 1974.

12. Mechanical Technology Incorporated Report MTI-75TR19, Acoustic Emission Detection of Fatigue Crack Initiation and Propagation in Notched and Unnotched Titanium Specimens, by Darlow, M.S., Shinaishin, O.A., and Aquaviva, S.J., pp. 7-10, January 1975.

13. Wadin, J.R., and Dunegan, H.L., "The Use of Spatial Filtering and Distribution Analysis of Acoustic Emission Signals to Isolate and Characterize Subcritical Crack Growth," The Third Acoustic Emission Symposium, Tokyo, Japan, pp. 183-193, Japan Industrial Planning Association, pp. 183-193, 1976.

14. Bailey, C.D., Hamilton, J.M., and Pless, W.M., "AE Monitoring of Rapid Crack Growth in a Production-size Wing Fatigue Test Article," NDT International, Vol. 9, No. 6, pp. 298-304, December 1976.

15. Lindley, T.C., Palmer, I.G., and Richards, C.E., "Acoustic Emission Monitoring of Fatigue Crack Growth," Materials Science and Engineering, Vol. 32, No.1, pp. 1-15, January 1978.

16. Peapel, P.N. and Topp, K., "Acoustic Emission - an Analytical System for Research and Teaching," Metallurgist and Materials Technologist, Vol. 14, No. 1, pp. 21-24, January 1982.

17. Provan, J.W., "The Micromechanics of Fatigue Crack Initiation," Proceedings of the Tenth Canadian Fracture Conference, Waterloo, Ontario, Canada, pp.131-154, Martinus Nijhoff Publishers, 1984.

18. Bathias, C., "The Use of Experimental Techniques for Description of Fatigue Damage," Subcritical Crack Growth Due to Fatigue, Stress Corrosion and Creep, pp. 84-106, Elsevier Applied Science Publishers, 1981.

19. Houssny-Emam, M. and Bassim, M.N., "Study of the Effect of Heat Treatment on Low Cycle Fatigue in AISI 4340 Steel by Acoustic Emission," Materials Science and Engineering, Vol. 61, No. 1, pp 79-88, October 1983.

20. Bouksim, L. and Bathias, C., "Initiation and Propagation of Short Cracks in and Aluminum Alloy Subjected to Programmed Block Loading," The Behaviour of Short Fatigue Cracks, pp. 513-526, Mechanical Engineering Publications, 1986.

21. Air Force Wright Aeronautical Laboratories Report
     AFWAL-TR-88-3008,Automated Early Fatigue Damage Sensing,
     by Hencken, A. and Horn, M., pp. 56, March 1988.

22. Gorman, M.R., "Plate Wave Acoustic Emission" submitted to
     Journal of the Acoustical Emission Society of America, 1990.

23. Graff, K.F., Wave Motion in Elastic Solids, pp. 229-236, Ohio
     State University Press, 1975.

24. Achenbach, J.D., Wave Propagation in Elastic Solids, pp.
     257-258, American Elsevier Publishing Co., 1973.

25. Spotts, M.F., Design of Machine Elements, pp. 87-95,
     Prentice-Hall, Inc., 1978.

26. Hsu, N.N. and Hardy, S.C., "Experiments in Acoustic Emission
     Waveform Analysis for Characterization of AE Sources, Sensors
     and Structures," Elastic Waves and Non-Destructive Testing of
     Materials, pp. 86-106, The American Society of Mechanical
     Engineers, 1978.

INITIAL DISTRIBUTION LIST

1. Defense Technical Information Center   2
    Cameron Station
    Alexandria, VA   22304-6145

2. Library, Code 52   2
    Naval Postgraduate School
    Monterey, CA   93943-5002

3. Commander   1
    Naval Air Systems Command
    Attn: E-2C Class Desk
    Naval Air Systems Command Headquarters
    Washington, D.C.   20361-0002

4. Dr. M. A. Hamstad   1
    Department of Engineering
    University of Denver
    Denver, CO   80208-0177

5. Dr. Joseph S. Heyman   1
    Mail Code: 231
    Langley Research Center
    Hampton, VA   23665-5225

6. Dr.George Sandeckyj   1
    WRDC/FIBEC
    WAFB, OH   45433-6553

7. Dr. William R. Scott   1
    Code 6063
    Naval Air Development Center
    Warminster, PA   18974

8. Dr. Henry Chaskelis   1
    Code 6385
    Naval Research Laboratory
    Washington, D.C.   20375

9. Mr. Mark Laspia   1
    GASD, Grumman Aerospace Corporation
    Bethpage, NY 11714

10. Dr. Richard Friedman   1
    Mechanics Section, Grumman Aerospace Corporation
    Bethpage, NY 11714

11. Mr. Richard Chance   1
    QAT Section, Grumman Aerospace Corporation
    Bethpage, NY 11714